# Structure and ultrastructure of nuptial and extranuptial nectaries explain secretion changes throughout flower lifetime and allow for multiple ecological interactions

# Structure and ultrastructure of nuptial and extranuptial nectaries explain secretion changes throughout flower lifetime and allow for multiple ecological interactions

**Running Title:** Structure and ultrastructure of nuptial and extranuptial nectaries

Hannelise Balduino[1], Priscila Tunes[2], Massimo Nepi[3,4], Elza Guimarães[2], Silvia Rodrigues Machado[2,5]

[1]Postgraduate Program in Plant Biology, São Paulo State University, Brazil.
[2]Department of Biodiversity and Biostatistics, Laboratory of Ecology and Evolution of plant-animal interactions, Institute of Biosciences, São Paulo State University, Botucatu, Brazil.
[3]Department of Life Sciences, University of Siena, Siena, Italy
[4] National Biodiversity Future Centre (NBFC), Palermo, Italy
[5]Microscopy Center of the Institute of Biosciences of Botucatu, São Paulo State University, Botucatu, Brazil.

Corresponding authors e-mail: elza.guimaraes@unesp.br ; silvia.machado@unesp.br

**Abstract**

Nectaries are specialized nectar-producing structures. Nectar traits affect animal behaviour and ecological and evolutionary processes, such as pollination and biotic defence. We previously found that there are differences in the characteristics of nuptial and extranuptial nectar and in the types of animals that visit each nectary in *Amphilophium mansoanum* (Bignoniaceae) flowers. We now hypothesize that nectar traits reflect the anatomical, histochemical, and subcellular characteristics of each nectary type. Using routine light microscopy, scanning electron microscopy, and transmission electron microscopy methods, we studied nuptial and extranuptial nectaries (NN and ENN, respectively) in young flower buds, pre-anthesis buds, and first- and second-day flowers. NN was a prominent annular disk, whereas ENN was a concave, patelliform trichome. Only ENN contained alkaloids, while both nectaries contained starch grains, lipid droplets, proteins, terpenes and phenolic compounds. Both nectaries showed subcellular organization consistent with hydrophilic and lipophilic secretion, the latter being predominant in second-day flowers. In NN, the subnectary parenchyma had phloem and amyloplasts until pre-anthesis. Starch grains decreased and tracheary elements were seen in newly opened flowers. ENN are not vascularised, with vascular bundles from the calyx approaching the base of the nectary. Starch grains were scarce and very small in the ENN secretory head cells. Fibrillary proteins were found only in NN and periplastidial reticulum was observed only in ENN. In NN, nectar secretion begins shortly before anthesis, being released through the raised stomata and the reticulate cuticle. In ENN, secretion extends from the young flower bud stage to senescent flowers, accumulating in small subcuticular spaces and being continuously released through the intact cuticle. Temporal differences in nuptial and extranuptial nectar production, as well as in the structural characteristics and nectar release mechanisms between nuptial and extranuptial nectaries, may explain the differences in nectar characteristics of *A. mansoanum*.

**Key words**: ant, bees, extranuptial nectary, mutualism, nuptial nectary, ultrastructure.

## Introduction

Nectar, a sugar-rich secretion, is a highly energetic and ready-to-consume primary resource for several animals (Nepi *et al.* 2018; Nicolson 2007, 2022). When these animals forage among different plant species, they come across nectar with different volume,

chemical profiles (including sugars, amino acids, proteins, lipids, organic acids and secondary compounds), and concentrations (Calixto *et al.* 2021; Barberis *et al.* 2023; Zhou *et al.* 2024). Due to the effects of these traits on animal's foraging behaviour and movement, nectar is an important mediator of mutualisms between plants and animals, including pollination and indirect defence against herbivores (Nicolson 2007, 2022; Heil 2015; McPeek *et al.* 2021; Mogensen *et al.* 2024). When plants and animals exert selective pressures on each other, these interactions can either increase or decrease reproductive and survival success, thereby affecting ecological and evolutionary processes (Nepi 2017; Nepi *et al.* 2018; Suissa *et al.* 2024).

Nectaries, *i.e.*, structures specialized in nectar production, show a wide range of sizes, morphology, anatomy, and locations (Erbar 2014 and references therein), which may influence nectar traits (Petanidou *et al.* 2000; Nepi 2007). Based on their topography, they are further categorized as floral or extrafloral nectaries (Caspary 1848). From a functional perspective, nectaries can be classified as nuptial, when associated with pollination, or extranuptial, when associated with defence (Delpino 1873).

Considering that nectaries have evolved independently across angiosperms (Weber and Keeler 2013; Phukela *et al.* 2020), including different lineages of Bignonieae (Bignoniaceae) (Nogueira *et al.* 2013), and the cost of nectar production for plants (Southwick 1984; Pyke 1991), it is expected that mechanisms of nectar synthesis and release would be variable among plant organs (Nepi 2007; Chatt *et al.* 2021) and flower developmental stages (Nepi 2007; Guimarães *et al.* 2016). Besides that, traits such as vascularisation, may severely affect nectar traits (Frey-Wyssling 1955; Galetto 1995). Therefore, studying nectary micromorphology, anatomy, and ultrastructure is essential to understand the relationships between plants, visiting animals, and the environment (Kostryco and Chwil 2022; Almeida *et al.* 2023).

Members of the Bignoniaceae family, including *Amphilophium mansoanum* (DC.) L.G. Lohmann [sin. *Distictella mansoana* (Vahl) Urb.], commonly have two nectary types in the same species, nuptial and extranuptial, which are usually morphologically different (Galetto 1995; Balduino *et al.* 2023) and have distinct evolutionary origins (Lohmann and Taylor 2014). Nuptial nectaries are typically annular disks at the ovary base (Thomas and

Dave 1992; Galetto 1995, 2009; Bernardello 2007; Rivera 2000a; Guimarães *et al.* 2016, 2018), composed of a unistratified epidermis, nectary and subnectary parenchyma supplied with phloem (*sensu* Nepi 2007). Their secretion begins before anthesis, so that nectar is already available when a flower opens (Guimarães et al. 2016, 2018). Nectar-secreting cells contain abundant mitochondria, rough endoplasmic reticulum, Golgi bodies with numerous vesicles, and amyloplasts, which degrade as anthesis progresses (Guimarães *et al.* 2016, 2018; Machado *et al.* 2017). Secretion may shift from hydrophilic to lipophilic during anthesis, which is distinguished by an increase in plastoglobuli, and is released through modified stomata, cuticular pores, or microchannels (Machado *et al.* 2016; Guimarães *et al.* 2016, 2018). In contrast, extranuptial nectaries are glandular trichomes that vary in shape, size, number, and location (Seibert 1948; Rivera 2000b; Nogueira *et al.* 2013; Fróes *et al.* 2015; Miranda *et al.* 2024). These trichomes are composed of a stalk and a multicellular secretory head, with cells showing abundant mitochondria, endoplasmic reticulum, leucoplasts, few dictyosomes, and wall ingrowths with plasmodesmata between the stalk and the secretory head cells (Gama *et al.* 2016). Different types of nectar-secreting trichomes (putative nectaries) may occur adjacently on the same perianth whorl (Elias and Gelband 1976; Galetto 1995; Nogueira *et al.* 2013; Fróes *et al.* 2015).

In a previous study with *A. mansoanum*, two types of nectaries were found within a given flower, nuptial (annular disk) and extranuptial (patelliform glands near the calyx margins), which nectar differs in composition, volume, concentration, and secretion dynamics (Balduino *et al.* 2023). Furthermore, since nuptial nectaries are visited by medium and large bees, while extranuptial nectaries are visited mainly by ants. Nectar from both nectary types differed regarding chemical composition, being nuptial nectar sucrose-dominated and extranuptial nectar hexose-rich, the first had a more variable amino acid profile than the latter and had a theophylline-like alkaloid, which was exclusive from nuptial nectar (Balduino *et al.* 2023).

While this previous study focused on the ecological and chemical aspects of nectar, in this research we aim, to expand upon those findings by investigating the anatomy, ultrastructure and histochemistry of the nuptial and extranuptial nectaries that co-reside in *A. mansoanum* flowers from a developmental perspective. Studying the structure and functioning of the different nectaries within a given flower expands our understanding on the

relationships between nectaries and their secretions, which mediate plant-animal interactions. We hypothesize that the specificities of nectar from nuptial and extranuptial nectaries of *A. mansoanum* (shown in Balduino *et al.* 2023) reflect underlying subcellular specializations. Beyond that, nectaries that coexist within the same flower are subjected to the same environmental and physiological conditions. Therefore, by comparing the structural mechanisms that govern the nectar secretion process in distinct nectaries and their respective functioning, we can gain deeper insights into how nectary features relate to their ecological functions.

## Material and Methods

*Plant material and study site*

*Amphilophium mansoanum* is a liana native to Brazil but not endemic, exhibiting a broad geographic distribution across the country, particularly on the edges of tropical forests and savannas (Lohmann and Taylor 2014). The zygomorphic, pentamerous flowers are arranged in racemose panicles, although simple racemes may occasionally occur (Pool, 2009) (Fig. 1A). The dome-shaped calyx is coriaceous with a cluster of glands near its margins (Fig. 1B). The corolla is infundibuliform, bent at ca. 90° above the base, coriaceous, with five lobes, imbricate, white and internally yellow (Fig. 1A). The androecium has four stamens and included anthers. The ovary is sessile, and the nectary disk is annular (Fig. 1C). Drops of viscous secretion (Fig.1 D) occur on the calyx surface from young floral buds to open flowers.

We sampled flowers (n= 3 flowers per stage, 4 plants) at four different stages of development: young buds (10-20 mm), pre-anthesis buds (40-50 mm), freshly opened flowers (first-day flowers) and flowers around 24 hours from opening (second-day flowers). The samples of the nuptial nectary (NN) and extranuptial nectary (ENN) were collected in the morning hours from natural populations of *A. mansoanum* at the edge of cerrado vegetation in the Midwest of São Paulo State, Brazil (22°53′56″S and 48°29′68″W; 966 m), from November 2021 to February 2023. A voucher specimen was deposited at the BOTU herbarium (Águas de Santa Bárbara, São Paulo, Brazil) under number 41575. The collection was made by T.C. Monteiro and H.K. Balduino.

*Structural, histochemical and ultrastructural studies*

For general histological characterization, samples were fixed in 2.5% glutaraldehyde in 0.025 M phosphate buffer (Feder and O'Brien 1968) in field conditions and maintained overnight at 4°C in the laboratory. Specimens were dehydrated through graded series of ethanol solutions (60-100%), and embedded in glycol methacrylate historesin (Leica Microsystems, Nussloch/Heidelberg, Germany). Thin sections (4-6 μm) were obtained using a semiautomatic microtome (Leica RM2245), placed on microscopic glass slides, stained with 1% toluidine blue in 1% aqueous sodium tetraborate solution (O'Brien *et al.* 1964) and mounted in synthetic resin (Entellan, Merck KgaA, Darmstadt, Germany). The results of the light microscopic examinations were documented with a photomicroscope (Leica DMR) equipped with a digital camera (Leica DFC 500).

For histochemical studies, fresh NN and ENN samples were hand-cut using a razor blades and subjected to the following treatments: Alcian blue for polysaccharides and acid polysaccharides (Figueiredo *et al.* 2007); Lugol's reagent for alkaloids and starch grains (Johansen 1940); ferric chloride for phenolic compounds (Johansen 1940); mercuric bromophenol blue for proteins (Mazia *et al.* 1953); NADI reagent (α-naphthol + dimethyl-p-phenylenediamine) for essential oils and oleo-resins (David and Carde 1964); ruthenium red for pectin (Jensen 1962); and Sudan IV for total lipids (Johansen 1940). When required, standard control sections were prepared at the same time. All observations and documentation were performed using a light microscope (Leica DMR) with a digital camera (Leica DFC 500).

For surface examination, portions of the flowers were cut with razor blades in the median longitudinal and transversal planes. The samples were fixed in 2.5% glutaraldehyde (0.1 mol. $L^{-1}$ phosphate buffer, pH 7.2), dehydrated in an aqueous ethanolic series, critical-point dried (Bal-Tec CPD 030), mounted on a metallic support with adhesive, and sputtered coated with gold (10 nm) (Bal-Tec SCD 050) following Bozzola and Russel (1992). The material was then examined with a scanning electron microscope (SEM Quanta 200, Fei Company, FEI, Gräfelfing, Germany) at 20 kV.

For cellular ultrastructure examination, the fragments were fixed in 2.5% glutaraldehyde (0.1 M sodium phosphate buffer pH 7.3, overnight at 4° C) and post-fixed with 1% osmium tetroxide ($OsO_4$) in the same buffer for 2 h at room temperature (Hayat

1989). After washing in distilled water, the material was dehydrated in aqueous acetone and embedded in Araldite resin (Araldite 502, Electron Microscopy Sciences, Hatfield, USA). Semi-thin sections (0.5 μm) were obtained using an ultramicrotome (Leica Reichert) and stained with 0.05% toluidine blue (O'Brien *et al.* 1964). Ultrathin sections (60 nm) were stained with 2% uranyl acetate solution for 15 min and lead citrate for 15 min (Reynolds 1963) and observed with a transmission electron microscope (TEM Tecnai Spirit, FEI Company, Germany) at 60 kV.

We also employed the zinc iodide–osmium tetroxide (ZIO) method for endomembrane impregnation (Reinecke and Walther 1978). After primary fixation, the samples were incubated in a solution containing Zn, I, TRIS-aminomethane and 1.0% osmium tetroxide (Reinecke and Walther 1978), and processed conventionally for TEM.

## Results

*Nuptial nectary structure, ultrastructure and secretion*

The nuptial nectary (NN) is an annular disk located below the ovary (Fig. 1C, 2A). The expanded base of the stamen filaments creates a constriction that surrounds the nectary and forms a nectar chamber (Fig. 1C), where the secreted nectar builds up. Nectar secretion begins in pre-anthesis floral buds. At this developmental stage, nectary surface had common epidermal cells with different sizes and shapes, with anticlinal walls that were undulating to different degrees and external periclinal walls sticking out (Fig. 2B-C). Numerous stomata also with different shapes and sizes were distributed across the surface of the nectary (Fig. 2B-C). The curvature of the external periclinal wall varied from flat to slightly convex to rounded (Fig. 2C). These included ordinary stomata with a long narrow opening and an outer stomatal rim, as well as stomata that were sunken or raised (Fig. 2B-C). Giant and raised stomata with a large opening and stomatal border, elevated by their subsidiary cells, were commonly observed (Fig. 2D). First-day flowers showed flocculent secretion residues covering the nectary surface (Fig. 2E). At this point, the giant raised stomata had a bigger round opening that was full of secretion residues (Fig. 2F).

Cross-sections of the NN of pre-anthesis buds showed three different regions under a light microscope (Fig. 3A). They featured a single-layered epidermis, a nectary parenchyma situated beneath the epidermis, and a large subnectary parenchyma that was densely

vascularised by vascular bundles originating from the flower receptacle (Fig. 3A). At this stage, a clear separation of the nectary and subnectary parenchyma was evident (Fig. 3A): the nectary parenchyma was made up of conspicuous cells with an ovoid to isodiametric shape that were arranged in 3-5 nonvascularised parenchymal layers (Fig. 3B); the subnectary parenchyma was made up of ovoid cells that were arranged in several layers with proliferating vascular bundles, mostly phloem (Fig. 3C). On the first day of anthesis, flowers had an increase in voluminous starch grains in the subnectary parenchyma cells (Fig. 3D), while in the nectary parenchyma, the intercellular spaces developed and were filled with secretions (Fig. 3E). Stomata with large open pores are evident at this stage (Fig. 3F). On the second day of anthesis, the epidermal cells and parenchyma cells displayed dense accumulations (Fig. 3G-H), while the starch grains were either absent or scarce (Fig. 3I). At this stage, parenchyma cells contained homogenous content (Fig. 3I), probably phenolic compounds, and tracheary elements in the subnectary parenchyma (Fig. 3J).

The histochemical characterization of the disk tissues of first-day flowers revealed positive reaction for hydrophilic and lipophilic substances (Fig. 4; Table 1). Tests with mercury blue bromophenol detected basic proteins stained in blue in the subnectary parenchyma cells, mainly in the vascular bundles (Fig. 4A), and in nectary parenchyma cells (Fig. 4 B). Alcian blue highlighted acid polysaccharides substances (Fig. 4C). Tests with NADI reagent also showed a positive result, developing both a pink coloration (characteristic of oil-resins) and a blue colouration (characteristic of essential oils) in the parenchyma cells (Fig. 4D). Tests with Lugol revealed accumulation of big starch grains in all disk tissues, but more numerous in the subnectary parenchyma (Fig. 4E). Tests with Sudan IV stained in red lipid droplets (Fig. 4F) and accumulations of lipid material in the intercellular spaces (Fig. 4G). With ferric chloride, all the nectary cells were stained brown (Fig. 4H), indicating the presence of phenolic substances. Tests with ruthenium red stained mainly cell walls (Fig. 4I).

Under TEM, NN epidermal cells of the pre-anthesis buds displayed thick external periclinal walls covered by a thin cuticle (Fig. 5A). There were a lot of free ribosomes, mitochondria, plastids (Fig. 5B-C) and rough endoplasmic reticulum with cisternae and vesicles filled with dense content, which was marked by ZIO (Fig. 5C). Amyloplast containing starch grains and leucoplasts with dense matrix devoid of inner membranes and containing a large osmiophilic inclusion occurred side by side in the epidermal cell (Fig. 5B).

The cytosol displayed oil drops (Fig. 5A, C). The vacuoles contained osmiophilic inclusions and flocculent materials (Fig. 5C). Accumulations of similar materials also occurred within the periplasmic space (Fig. 5A-C). In the nectary parenchyma (Fig. 5D-F), the cells exhibited compact arrangement, thin walls, large nuclei, and vacuoles of varied sizes (Fig. 5D), along with amyloplasts exhibiting different sizes and signs of degradation (Fig. 5E). These cells regularly displayed leucoplasts containing small starch grains and osmiophilic globules (terpenes/oils/phenols) (Fig. 5F). Inside the vacuoles, flocculent contents and membrane debris were observed (Fig. 5D, F). In the subnectary parenchyma, the cells were larger and contained numerous amyloplasts (Fig. 5G-I), as well as prominent nucleus (Fig. 5I). The vacuoles varied in size and contained flocculent materials (Fig. 5H-I). The intercellular spaces were filled with flocculant materials (Fig. 5I). Plasmodesmata were seen in the regions of contact between parenchyma cells (Fig. 5H). At this stage, the phloem was the main vascular tissue in the subnectary parenchyma (Fig. 5J), with sieve tube elements displaying a wide calibre (Fig. 5K), and parenchyma cells showing amyloplasts with voluminous starch grains (Fig. 5L).

The nuptial nectaries of first-day flowers contained epidermal cells characterized by large vacuoles at the distal pole (Fig. 6A) and densely granulated cytoplasm (Fig. 6B). Amyloplasts were localized at the base of the epidermal cells and were characterized by very electron-dense stroma and broken-down starch grains (Fig. 6A). Lipid droplets occurred dispersed in the cytoplasm and near the plasma membrane (Fig. 6B). The cuticle featured a large cuticular layer with a network of electron-dense ramifications that does not extend to the cuticle itself (Fig. 6C). This ultrastructural organization of the cuticle suggests a pattern resembling microchannels, through which secretion reaches the surface. Secretion residues were observed on the cuticle (Fig. 6C). At this stage, the nectary (Fig. 6D) and subnectary parenchyma (Fig. 6E) cells showed increased vacuolization and a higher number of amyloplasts, which consist of starch grains being broken-down. Small vacuoles were either juxtaposed or fused with larger vacuoles (Fig. 6D-E), which contained fibrillary or flocculated materials, membrane debris, and osmiophilic inclusions (Fig. 6E). Intercellular spaces were wider and filled with flocculant material (Fig. 6E). In the phloem parenchyma cells, signs of degradation were noted in the amyloplasts (Fig. 6F). Additionally, we observed sieve tube elements with callose-plugged sieve plates (Fig. 6F-G). In the cytoplasm of

phloem parenchyma cells, bundles of fibrillar protein were abundant, especially near the vacuoles (Fig. 6H). These cells had globular mitochondria, endoplasmic reticulum segments, dictyosomes, and ZIO marker-improved vesicles view (Fig. 6I).

In the nuptial nectary of second-day flowers, cytoplasm was reduced to a thin parietal layer, and a central vacuole had been formed in epidermal (Fig. 6J), nectary parenchyma (Fig. 6 K), and subnectary parenchyma cells (Fig. 6L). Amyloplasts (Fig. 6J) exhibited residual starch grains, dense stroma and large osmophilic inclusions (like terpenes/phenols). Subnectary parenchyma cells showed a big nucleus, larger vacuoles, and amyloplasts that were full of osmophilic substances (e.g. phenols and terpenes) and broken-down starch grains (Fig. 6L–M). These cells also exhibited segments of endoplasmic reticulum and mitochondria (Fig. 6M). Intercellular spaces were wider (Fig. 6L) and filled with flocculent material (Fig. 6N). Osmiophilic bodies were observed attached to the tonoplast (Fig. 6N).

*Extranuptial nectary structure, ultrastructure and secretion*

Under SEM, the secretion-producing areas on the calyx exhibited patelliform-concave glands surrounded by simple, uniseriate and pluricellular non-glandular trichomes with pointy apical cells and warty ornamentations, as well as peltate glandular trichomes featuring a flat head and raised stomata (Fig. 7A-C). The extended margins of the patelliform glands protruded above the calyx surface (Fig. 7B, D). Transversal sections through the gland revealed that the concave portion was aligned with the epidermis, while the foot was immersed in the calyx mesophyll (Fig. 7D). The glands of young buds (Fig. 7E-F) did not possess fully developed edges, but displayed three distinct areas: i) a concave, multicellular secretory head composed of very long, narrow, thin-walled cells covered with a thick cuticle; ii) a short stalk that extends for the length of the secretory head; and iii) a foot, or base, comprised of numerous tangentially expanded cells. A single layer of flattened, rectangular cells with thick anticlinal walls constitutes the stalk, connecting the secretory head to the nectary foot (Fig. 7E-F). The foot of the gland is not vascularised and consisted of 3-5 layers of cells with varied sizes and shapes, which contents are strongly stained with toluidine blue (Fig. 7E-F). Vascular bundles from the calyx mesophyll circumscribe the gland foot, but they do not extend through it (Fig. 8A).

In young buds, these glands are already secreting material despite the edges not being fully developed yet. The exudate was stored beneath the cuticle in the centre of their concave head (Fig. 7G). As differentiation progressed, the edge of the concave gland widened, and all gland cells, except for the stalk cells, became denser and more toluidine blue-stained (Fig. 7H). Progressively, the edges become more extended and the vacuoles in the head and foot cells become more developed (Fig. 7I) on first-day flowers. Additionally, the head secretory cells exhibit thicker walls. They possess a conspicuous nucleus with well-organized nucleolus, less cytoplasm, and several small vacuoles (Fig. 7J). The thick-walled cells in the gland stalk contained large a vacuole and reduced cytoplasm (Fig. 7J).

Histochemical analysis of mature ENN in first-day flowers revealed positive reaction for hydrophilic and lipophilic substances (Fig. 8; Table 1). With ferric chloride, phenolic substances were stained brown and were detected in all nectary cells (Fig. 8A), with a higher concentration in the gland's apex (Fig. 8B). After Sudan IV tests, the thick cuticle and lateral cell walls of the stalk were better delimited (Fig. 8C). These tests also revealed that head secretory cells (Fig. 8D) and foot cells (Fig. 8E) contained abundant lipid droplets. Basic proteins were abundant in the head cells (Fig. 8F). Oil-resins, typically stained in pink with NADI reagent, were also found in the head cells (Fig. 8E). With Lugol's reagent, small amounts of starch grains were detected in the head cells, whereas the contents of the foot cells acquired a reddish-brown colour (Fig. 8F), indicating the presence of alkaloids. Ruthenium red treatment evinced an abundance of pectin in the thick cell walls of the gland foot and of the central region of the secretory head (Fig. 8I).

From young floral buds to second-day flowers, ENN were active in secretion. Under TEM, the secretory head cells in young buds were featured with large nuclei with organized nucleoli, dense cytoplasm, poorly developed or absent vacuoles (Fig. 9A), and amyloplasts with abundant starch grains (Fig. 9B-C). ZIO reaction showed that the dictyosomes were well-developed and active in vesicle production (Fig. 9C). In pre-anthesis buds (Fig. 9D-I), the head cells had a lot of mitochondria and long rough endoplasmic reticulum profiles (Fig. 9D). Leucoplasts had residual starch grains and big osmiophilic inclusions (Fig. 9E). Elongated plastids devoid of inner membranes and presenting homogeneous stroma and periplastidial reticulum (Fig. 9F) were found in the head cells. Plasmodesmata were seen in the anticlinal walls connecting the secretory head cells (Fig. 9E-F). Golgi bodies cisternae

and vesicles with electron-dense material (Fig. 9G), marked by ZIO, were found in the head cells. Stalk cells had thicker lateral walls and very thin anticlinal walls (Fig. 9H). They also had large nuclei with evident nucleolus, dense cytoplasm with a lot of rough endoplasmic reticulum, and small vacuoles (Fig. 9H). Gland foot cells were tangentially expanded and had small vacuoles with dark inclusions, as well as cytoplasmic oil bodies (Fig. 9I).

In first-day flowers, cuticle was thicker and contained accumulations of lipids and an electron dense material (Fig.10A). The nuclei were central and spherical, with abundant cytoplasm displaying large lipid droplets (Fig. 10B). At this stage, there were periplasmic spaces and paramural bodies along the anticlinal walls (Fig. 10C), which exhibited areas with lipid inclusions (Fig. 10D). These cells contained polymorphic plastids with finely granular stroma and osmiophilic inclusions (Fig. 10E), likely terpene/phenols. In stalk cells, there were also lipid bodies, mitochondria, and small vacuoles (Fig. 10F). In the gland foot, intercellular spaces increased in size and were filled with flocculent material (Fig. 10G). In foot cells, the vacuoles were small, contained electron-dense bodies (Fig. 10G) and numerous mitochondria (Fig. 10H). In the secretory head of second-day flowers there were more dark cells (Fig. 10I) when compared to the previous stage (Fig. 10A). In addition, large accumulations of electron dense material were visible in the cuticle (Fig. 10I-J). The dark cells contained abundant cytoplasm with intact organelles and small vacuoles (Fig. 10K), globose mitochondria, well-developed Golgi bodies with numerous cisternae, sparse profiles of endoplasmic reticulum, and oil bodies (Fig. 10L).

## Discussion

The location and morphology of the nectary disk (nuptial nectary, NN) of *A. mansoanum* follow the pattern observed in other Bignoniaceae species (Gentry 1974; Elias and Gelband 1976; Galetto 1995; Rivera 2000; Guimarães *et al.* 2016; Frazão *et al.* 2020), as do the location and morphology of patelliform-concave glands (extranuptial nectary, ENN), as reported in different Bignoniaceae taxa (Subramanian and Inamdar 1985; Galetto 1995; Rivera 2000b; Díaz-Castelazo 2005; Nogueira *et al.* 2013; Gama *et al.* 2013; Fróes *et al.* 2015 ). The morphology and anatomy of the annular disks of *A. mansoanum* flowers aligns with the pattern suggested by Nepi (2007), being featured with uniseriate epidermis, nectary

parenchyma, and a wider densely vascularised subnectary parenchyma. The patelliform glands in *A. mansoanum* flowers have extended margins that project above the calyx surface.

Both nectaries exhibit cellular apparatus typical of nectar secretion; however, NN and ENN display distinct structural characteristics, which likely lead to varied nectar features (volume, concentration, and chemical composition).

Patelliform glands of *A. mansoanum* have a complex structure consisting of three specialized regions: nonvascularised foot, stalk, and secretory head. For some authors, such glands represent a symplesiomorphy of the group and are derived from peltate trichomes, showing similar anatomical structure, but different shapes, differential proliferation and cell expansion (Rivera 2000b; González 2013; Nogueira *et al.* 2013). Moreover, their stalk layers are considered an equivalent feature, differentiated by cell number and shape and by the number of cell layers (Fróes *et al.* 2015; Machado and Rodrigues 2021).

Similarly to other Bignoniaceae species (Machado *et al.* 2016; Guimarães *et al.* 2016, 2018), we saw changes in NN and ENN ultrastructure along flower development. These changes likely contribute to the differences in nuptial and extranuptial nectar traits of *A. mansoanum* recorded by Balduino *et al.* (2023).

Nuptial and extranuptial nectaries showed a significant difference in their sugar sources. In NN, starch grains, stored in the parenchyma cells during flower lifetime, are depleted during the pre-anthesis stage and on the first day of anthesis, as reported by Pacini *et al.* (2003). This information associated with NN vascularisation indicates that NN can get their energy directly from the phloem. In tun, starch grains are absent or present in minimal amounts in ENN. Thus, the nectar sugar may originate directly from photosynthesis within the nectary or from the calyx tissues surrounding the gland foot, as described in nonvascularised nectaries (Nepi 2007). It is noticeable that the foot cells of the patelliform glands (immersed in the calyx mesophyll) have more abundant plasmodesmata when compared to other gland regions. The calyx's vascular tissues end at the base of the gland, and do not penetrate the foot of the gland. Pre-nectar likely exits the sieve tubes through an apoplastic route via intercellular spaces, reaches the gland foot, and follows a symplast route in an ascending Trajectory through plasmodesmata, reaching the stalk cells. The apoplasmic barrier in the lateral cell walls of the stalk cells directs the pre-nectar towards the secretory head (Fahn 1979; Machado and Rodrigues 2021). In *A. mansoanum*, there is a substantial

difference in nectar volume between the two types of nectaries (Balduino *et al.* 2023). Although this is not a general rule, this pattern is consistent with what has been reported by Díaz-Castelazo *et al.* (2005) for other ENN, as NN are directly vascularised, while ENN are smaller and nonvascularied. However, the clustered ENN, considered an adaptative trait (Elias and Newcombe 1979), may collectively produce enough nectar to ensure ant visitation to the calyx surface.

It is noticeable that the development level of the phloem and xylem in NN varies between pre-anthesis buds and open flowers, with a predominance of phloem in pre-anthesis buds. During this stage, phloem was characterized by large-calibre sieve tubular elements, indicating that non-reducing sugars (and other solutes) are being unloaded into the subnectary parenchyma where they will be stored as starch grains (Taiz *et al.* 2013). In most Bignoniaceae species, nuptial nectary is supplied by phloem elements, except for *Tabebuia heptaphylla* (Vellozo) Toledo, in which they are vascularised by both xylem and phloem (Galetto 1995). A correlation between nectar concentration and nuptial nectary vascularisation was highlighted by Frey-Wysling (1955) but remains poorly investigated. Our study demonstrated that the nuptial nectary of *A. mansoanum* is vascularised with phloem and xylem. The appearance of tracheary elements in the subnectary parenchyma of first-day flowers indicates a change in the translocation route and pre-nectar components, which is common depending on the stage of organ development and on the vascular connections between source and sink (Taiz *et al.* 2013). This change means that water, supplied both by phloem and xylem, is being used to compose nectar, which may result in a more diluted secretion with lower sugar concentration. This is consistent with the characteristics of *A. mansoanum* nuptial nectar reported by Balduino *et al.* (2023), which was found to be less concentrated and more abundant than that of other Bignonieae species (Galetto 1995, 2009). Both bee pollinator species reported visiting *A. mansoanum* flowers are from the Centridini tribe (Yanagizawa and Gottsberger 1982; Balduino *et al.* 2023). Although they prefer nectar with higher sugar concentrations (Roubik *et al.* 1995), it's possible that they can use physiological and behavioural adaptations to concentrate diluted nectar (Nicolson 2009), which may allow them to explore a wider range of nectar concentrations (Galetto 2009), as well as different volumes.

The flowers of *A. mansoanum* quickly release a lot of nuptial nectar (Balduino *et al.* 2023). This might happen because of the large amyloplasts in the parenchyma cells, which differentiate before secretion and lose most of their starch grains. Thus, starch grains were either used to make nectar sugars or to provided energy for the secretory process (Fahn and Shimony 2001; Stpiczyńska *et al.* 2005; Heil 2011; Guimarães *et al.* 2018). Based on a disk surface SEM study, it appears that the modified and raised stomata of *A. mansoanum* primarily facilitate nectar release (Gaffal *et al.* 1998; Wist and Davis 2006; Tölke *et al.* 2015). TEM examination of the cuticle that cover the disk epidermis revealed a reticulated structure, which may enhance permeation and facilitate the release of fat-soluble substances (Paiva 2016, 2017). The observation of secretion residues on the cuticle adds to the evidence that lipophilic components of secretion are also being released through microchannels. Ascensão *et al.* (1997) suggested that microchannels constitute the exit route of volatile substances. On the other hand, secretion accumulates in small subcuticular spaces in patelliform glands, particularly within the central epidermal cells, and is released through the cuticle or small pores. These findings suggest that extranuptial nectar release occurs continuously, while nuptial nectary releases secretion all at once through raised stomata. These findings align with the variation of nuptial and extranuptial nectar production in space and time. Nuptial nectary has a short lifespan and is active in secretion from pre-anthesis buds to second-day flowers, while extranuptial nectary is active from young buds to senescent flowers, and apparently to young fruits.

In general, the ultrastructural organization of the epidermal secretory cells in both NN and ENN is made up of a complex system of endomembranes, including the endoplasmic reticulum, dictyosomes, and vesicles. Dictyosomes in the gland cells are associated with the production of hydrophilic substances, while free ribosomes and rough endoplasmic reticulum elements can be related to the synthesis of enzymes involved in starch grain hydrolysis and degradation processes, which were observed during nectar secretion (Paiva and Machado 2008; Possobom *et al.* 2010; Tölke *et al.* 2015; Guimarães *et al.* 2016, 2018). However, the nectaries of *A. mansoanum* differ in abundance and volume of amyloplasts, mitochondria, oil droplets, and degree of RER development. Moreover, the presence of fibrillar proteins was observed only in NN, while plastids with periplastidial reticulum were observed only in ENN. Recent findings highlight how mitochondria, along with plastids and the cytosol, help

produce terpenes (Pazouki and Niinemets 2016). Thus, the increase in number of mitochondria observed here can be indicative of their involvement in terpene synthesis in NN. The increase in the presence of lipids is commonly reported throughout nectary development (Tölke *et al*. 2015; Guimarães *et al*. 2016, 2018). The presence of oil droplets in vacuoles, scattered throughout the cytosol and within the periplasmic spaces, which are more abundant in ENN than in NN, is ultrastructural evidence of lipidic secretion (Canaveze *et al.* 2021; de Deus Bento *et al.* 2024). Plastid morphology in the secretory cells is quite similar to that of plastids involved in the synthesis of terpenes/phenol in lipophilic glands (Kowalkowska *et al.* 2012, 2015; Machado *et al.* 2023), but is uncommon in nectariferous tissues (Guimarães *et al.* 2018). Numerous studies have indicated that plastids are involved in the synthesis of volatile compounds, primarily of phenolic and terpenoid compounds (Pridgeon and Stern 1985; Stern *et al.* 1987; Pais and Figueiredo 1994; Kowalkowska *et al.* 2012; Stpiczyńska and Davies 2016; Wiśniewska *et al.* 2018; Guimarães *et al.* 2018). The presence of polymorphic plastids containing lipophilic inclusions provides strong evidence that these structures are involved in scent production (Antón *et al.* 2012; Kowalkowska *et al.* 2015; Guimarães *et al.* 2018). Additionally, periplastidial reticulum contributes to the translocation and/or temporary concentration of lipophilic secretions (Sá-Haiad *et al.* 2015; Canaveze *et al.* 2021). It's possible that the osmium tetroxide-darkened material in the plastids, cytoplasm, RER, and vacuoles is made up of unsaturated lipids, terpenes, and phenolic compounds (Kowalkowska *et al.* 2015; Naczk *et al.* 2018), since osmium tetroxide is known to have better penetration properties and a strong affinity for double bonds (Angermuller and Fahini 1982). This is consistent with our histochemical tests that revealed lipids, terpenes, and phenolic compounds in the secretory cells. Despite the low specificity of the histochemical tests, Sudan IV and NADI reagent have been widely used to, respectively, locate total lipids and terpenes in secretory tissues (Figueiredo *et al.* 2007). Lugol's reagent, containing potassium iodide, can mark alkaloids in plant cells, in addition to staining starch grains (Figueiredo *et al.* 2007).

In NN, the presence of polysaccharides throughout the nectary, in cell walls and cytoplasm, keeps the tissue hydrated and may facilitated pre-nectar transport through nectary cells. As in NN, polysaccharides may also be related to nectar pathways in ENN. Their presence in the secretory head may also contribute to the viscosity of nectar (Fahn and

Benouaiche 1979), which is a feature that affects ant foraging behaviour (Lois-Milevicich *et al*. 2021) and may be related to the protection of nectar from desiccation and pathogens. Additionally, although further investigation is needed, polysaccharides could modulate volatile organic compound (VOC) liberation due to their distinct lipophilic nature. Thus, this could be an ecologically relevant feature, as ants rely on chemical cues for their activities (Knaden and Graham 2016; Nelson *et al.* 2019).

Both types of nectaries produce hydrophilic and lipophilic secretion at different developmental stages as reported in other bee-pollinated Bignoniaceae species (Baker 1977; Guimarães *et al.* 2018), which reveals the plastic potential of secretory cells. Some authors associate the presence of lipids to environmental conditions, since they may help prevent water loss and increase nectar's availability period (Cobert *et al*. 1979; Stpiczyńska *et al*. 2021; da Silva *et al*. 2025). Although this rationale applies to ENN, one can also interpret this result in terms of how valuable lipophilic compounds are for plants, as they can be floral scent compounds related to either attraction or repellence of animals, which may be mutualists or antagonists (Slavković and Bendahmane 2023). For animals, they can constitute part of dietary requirements that enhances their health (Barberis *et al.* 2023), movement (Gilbert *et al.* 1965; Levin *et al.* 2017), development and reproduction (Stone *et al.* 1985; Canavoso *et al.* 2001; Vaudo *et al.* 2015). Additionally, finding a source of nectar that contains lipids can benefit bees, such as *A. mansoanum* pollinators, that collect oil or mix oil with nectar to feed their larvae, since lipophilic compounds are more caloric than carbohydrates. Therefore, the presence of lipids and terpenes/phenols in both types of floral nectaries helps explain the diversity of animals with varying needs and ecological roles that visit *A. mansoanum* (Balduino *et al.* 2023).

Proteins are generally associated with plant defence (Schmitt *et al*. 2021) and their absence in ENN is a remarkable trait, since the proportion of protein amino acids in extranuptial nectar is higher than in nuptial nectar (Balduino *et al*. 2023). High enzyme activity could explain this result, especially because ENN is more subjected to microorganism arrival (Nepi *et al*. 2012). The presence of alkaloids in *A. mansoanum* nectary tissues is aligned with its nectar composition (Balduino *et al.* 2023) and may also protect against pathogens and antagonist herbivores (González-Teuber *et al*. 2009). Besides,

alkaloids also have neuroactive effects on visitors' foraging behaviour (Barberis *et al.* 2023; Mogonsen *et al.* 2024).

Nuptial nectaries suddenly release nectar right before anthesis starts, so when the flowers open, pollinators can immediately obtain nectar. This implies that the nectar volume available in nuptial nectaries is negatively linked to the number of bee visits received by a given flower, showing the ephemerality of this trophic resource associated to pollination mutualism. In contrast, extranuptial nectaries are active for a longer period of time. They produce nectar daily from the early bud stage until the flower dies, which may take up to six days (*unpublished data*). Even though nectar production stops in the afternoon (Balduino *et al.* 2023), extranuptial nectaries resume nectar production again early in the morning of the following day. This mechanism of long-lasting nectar production and secretion allows extranuptial nectaries to be explored by visiting insects for several days in a single flower, and even for several weeks, if one considers that there are floral buds in different stages within a given inflorescence.

## Conclusion

In *A. mansoanum*, nuptial and extranuptial nectaries coexist in the same flower and are exposed to similar environmental and physiological conditions. Both nectaries exhibit cellular apparatus typical of nectar secretion; however, they also display distinct structural characteristics. These differences are especially clear when considering for how long each type of nectary secretes and the different groups of animals that visit each nectary. Thus, the changes in both nuptial and extranuptial nectary cellular machinery through flower lifetime reflect the functioning of both nectaries, especially the duration of their secretory activity and the interactions in which each nectary type is involved. Therefore, understanding how the different nectaries within a flower function can enhance our comprehension of their ecological roles in mediating interactions between plants and animals.

## Data availability statement

The data underlying this article are available in the article.

## Conflict of Interest Statement

None declared.

**Acknowledgments**

We thank Marcos Benine for allowing us to collect the samples in his property; Dr. Daiane Maia de Oliveira for assistance in anatomical and histochemical analyses; Technicians of Electron Microscopy Center at the Institute of Bioscience (UNESP) for assistance in processing the materials and the provision of equipment for electron microscopy; Dr. Yve Canaveze for editing the figures. We also extend our thanks to the São Paulo Research Foundation (FAPESP) for financial support through the grant: #2021/10639-5 CBioClima - Center for Research on Biodiversity Dynamics and Climate Change.

**Funding**

This research was supported by the São Paulo Research Foundation (FAPESP - grant numbers #2018/14146-0 and #2009/17611-7 to E.G., and #2021/13392-0 to S.R.M.), National Council for Scientific and Technological Development (CNPq -grant numbers 308982/2020-7 to S.R.M.; 312799/2021-7 to E.G.; and PIBIC 45947 and to H.K.B.), and Coordination for the Improvement of Higher Education Personnel (CAPES—finance code 001) to the first author.

**References**

Almeida AL, Paiva EAS, Vieira MF, Ventrella MC. 2023. How can structure and nectar composition explain the secretory process in super productive nuptial nectaries of *Mabea fistulifera* Mart. (Euphorbiaceae)? *Protoplasma* 260:935–947.

Angermüller S, Fahimi HD. 1982. Imidazole-buffered osmium tetroxide: an excellent stain for visualization of lipids in transmission electron microscopy. *The Histochemical Journal* 14:823–835.

Anton S, Kaminska M, Stpiczynska M. 2012. Comparative structure of the osmophores in the flower of *Stanhopea graveolens* Lindley and *Cycnoches chlorochilon* Klotzsch (Orchidaceae). *Acta Agrobotanica* 65(2).

Ascensão L, Marques N, Pais MS. 1997. Peltate glandular trichomes of *Leonotis leonurus* leaves: ultrastructure and histochemical characterization of secretions. *International Journal of Plant Sciences* 158:249–258.

Baker HG. 1977. Non-sugar chemical constituents of nectar. *Apidologie* 8(4):349–356.

Balduino HK, Tunes P, Giordano E, Guarnieri M, Machado SR, Nepi M, Guimarães E. 2023. To each their own! Nectar plasticity within a flower mediates distinct ecological interactions. *AoB Plants* 15(2):plac067.

Barberis M, Calabrese D, Galloni M, Nepi M. 2023. Secondary metabolites in nectar-mediated plant–pollinator relationships. *Plants* 12:550.

Bernardello G. 2007. A systematic survey of floral nectaries. In: Nicolson SW, Nepi M, Pacini E, eds. *Nectaries and nectar*. Dordrecht: Springer, 19–128.

Bozzola JJ, Russel LD. 1992. Interpretation of microphotographs. In: *Electron Microscopy: Principles and Techniques for Biologists*. Jones and Bartlett Publishers, 377–404.

Calixto ES, Lange D, Bronstein J, Torezan-Silingardi HM, Del-Claro K. 2021. Optimal defense theory in an ant–plant mutualism: extrafloral nectar as an induced defence is maximized in the most valuable plant structures. *Journal of Ecology* 109(1):167–178.

Canaveze Y, Scudeler EL, Rodrigues Machado S. 2021. Neem secretory cells: developmental cytology and indications of cell autotoxicity. *Protoplasma* 258:415–429.

Canavoso LE, Jouni ZE, Karnas KJ, Pennington JE, Wells MA. 2001. Fat metabolism in insects. *Annual Review of Nutrition* 21(1):23–46.

Caspary R. 1848. *De nectariis*. Konigsberg: J. Schellhoff.

Chatt EC, Mahalim SN, Mohd-Fadzil NA, Roy R, Klinkenberg PM, Horner HT, Nikolau BJ. 2021. Nectar biosynthesis is conserved among floral and extrafloral nectaries. *Plant Physiology* 185:1595–1616.

Cobert SA, Willmer PG, Beament DM, Unwin DM, Prys-Jones OE. 1979. Post-secretory determinants of sugar concentration in nectar. *Plant Cell and Environment* 2:298–308.

da Silva Figueiredo AC, Barroso JM, Pedro LM, Ascensão L. 2007. Histoquímica e citoquímica em plantas: princípios e protocolos. Lisboa: Instituto de Investigação Científica Tropical.

da Silva MVO, Sfair JC, Loiola MIB. 2025. What's on the Menu? Floral Exudate Composition in Areas Subjected to Different Levels of Abiotic Severity. *Revista Brasileira de Geografia Física* 18(01):284–297.

David R, Carde JP. 1964. Histochimie-coloration differentielle des inclusions lipidiques et terpeniques des pseudophylles du pin maritime au moyen du reactif NADI. *Comptes Rendus Hebdomadaires des Seances de l'Academie des Sciences* 258:1338.

de Deus Bento KB, Canaveze Y, Machado SR. 2024. Oil and mucilage idioblasts co-occur in the vegetative organs of *Ocotea pulchella* (Lauraceae): comparative development, ultrastructure and secretions. *Protoplasma* 261(5):877–895.

Delpino F. 1873. Ulteriori osservazioni e considerazioni sulla dicogamia nel regno vegetale. *Atti della Società Italiana di Scienze Naturali* 16:151–349.

Díaz-Castelazo C, Rico-Gray V, Ortega F, Angeles G. 2005. Morphological and secretory characterization of extrafloral nectaries in plants of coastal Veracruz, Mexico. *Annals of Botany* 96:1175–1189.

Elias TS, Gelband H. 1976. Morphology and anatomy of floral and extrafloral nectaries in *Campsis* (Bignoniaceae). *American Journal of Botany* 63:1349–1353.

Elias TS, Newcombe LF. 1979. Foliar nectaries and glandular trichomes in *Catalpa* (Bignoniaceae). *Journal of Integrative Plant Biology* 21(3).

Erbar C. 2014. Nectar secretion and nectaries in basal angiosperms, magnoliids and non-core eudicots and a comparison with core eudicots. *Plant Diversity and Evolution* 131:63–143.

Fahn A, Shimony C. 2001. Nectary structure and ultrastructure of unisexual flowers of *Ecballium elaterium* (L.) A. Rich. (Cucurbitaceae) and their presumptive pollinators. *Annals of Botany* 87:27–33.

Fahn A. 1979. Ultrastructure of nectaries in relation to nectar secretion. *American Journal of Botany* 66:977–985.

Fahn A, Benouaiche P. 1979. Ultrastructure, development and secretion in the nectary of banana flowers. *Annals of Botany* 44(1):85–93.

Feder NED, O'Brien TP. 1968. Plant microtechnique: some principles and new methods. *American Journal of Botany* 55:123–142.

Figueiredo AC, Pais MSS. 1994. Ultrastructural aspects of the glandular cells from the secretory trichomes and from the cell suspension cultures of *Achillea millefolium* L. ssp. *millefolium*. *Annals of Botany* 74(2):179–190.

Frazão A, Lohmann LG, Costa ER, Demarco D. 2020. Structure of long-tubed white corollas: a case study from the trumpet-creeper family (Bignoniaceae). *Flora* 268:151598.

Frey-Wyssling A. 1955. The phloem supply to the nectaries. *Acta Botanica Neerlandica* 4:358–369.

Fróes FFPC, Gama TSS, Feio AC, Demarco D, Aguiar-Dias ACA. 2015. Structure and distribution of glandular trichomes in three species of Bignoniaceae. *Acta Amazonica* 45(4):347–354.

Gaffal KP, Heimler W, El-Gammal S. 1998. The floral nectary of *Digitalis purpurea* L., structure and nectar secretion. *Annals of Botany* 81:251–262.

Galetto L. 1995. Nectary structure and nectar characteristics in some Bignoniaceae. *Plant Systematics and Evolution* 196:99–121.

Galetto L. 2009. Nectary and nectar features: occurrence, significance, and trends in Bignoniaceae. *Journal of Plant Reproductive Biology* 1:1–12.

Gama TSS, Demarco D, Aguiar-Dias ACA. 2013. Ontogeny, histochemistry, and structure of the glandular trichomes in *Bignonia aequinoctialis* (Bignoniaceae). *Brazilian Journal of Botany* 36:291–297.

Gama TSS, Aguiar-Dias ACA, Demarco D. 2016. Transfer cells in trichomatous nectary in *Adenocalymma magnificum* (Bignoniaceae). *Anais da Academia Brasileira de Ciências* 88(Suppl 1):527–537.

Gentry AH. 1974. Coevolutionary patterns in Central American Bignoniaceae. *Annals of the Missouri Botanical Garden* 61:728–759.

Gilbert LI, Chino H, Domroese KA. 1965. Lipolytic activity of insect tissues and its significance in lipid transport. *Journal of Insect Physiology* 11(8):1057–1070.

Gonzalez AM. 2013. Indumento, nectarios extraflorales y anatomía foliar en Bignoniáceas de la Argentina. *Boletin de la Sociedad Argentina de Botanica* 48:221–245.

González-Teuber M, Heil M. 2009. Nectar chemistry is tailored for both attraction of mutualists and protection from exploiters. *Plant Signaling & Behavior* 4:809–813.

Guimarães E, Nogueira A, Machado SR. 2016. Floral nectar production and nectary structure of a bee-pollinated shrub from Neotropical savanna. *Plant Biology* 18:26–36.

Guimarães E, Tunes P, Almeida Junior LD, Di Stasi LC, Dötterl S, Machado SR. 2018. Nectar replaced by volatile secretion: a potential new role for nectarless flowers in a bee-pollinated plant species. *Frontiers in Plant Science* 9:1975.

Hayat MA. 1989. *Principles and Techniques of Electron Microscopy: Biological Applications*. 3rd edn. Boca Raton: CRC Press.

Heil M. 2011. Nectar: generation, regulation and ecological functions. *Trends in Plant Science* 16:191–200.

Heil M. 2015. Extrafloral nectar at the plant–insect interface: a spotlight on chemical ecology, phenotypic plasticity, and food webs. *Annual Review of Entomology* 60(1):213–232.

Jensen WA. 1962. *Botanical histochemistry: principle and practice*. San Francisco: W. H. Freeman.

Johansen P. 1940. Meister Michel Sittow Hofmaler der Königin Isabella von Kastilien und Bürger von Reval. *Jahrbuch der Preuszischen Kunstsammlungen* 61:1–36.

Knaden M, Graham P. 2016. The sensory ecology of ant navigation: from natural environments to neural mechanisms. *Annual Review of Entomology* 61(1):63–76.

Kostryco M, Chwil M. 2022. Nectar secretion, morphology, anatomy and ultrastructure of floral nectary in selected *Rubus idaeus* L. varieties. *Agriculture* 12:1017.

Kowalkowska AK, Kozieradzka-Kiszkurno M, Turzyński S. 2015. Morphological, histological and ultrastructural features of osmophores and nectary of *Bulbophyllum wendlandianum* (Kraenzl.) Dammer (*B. section Cirrhopetalum* Lindl., Bulbophyllinae Schltr., Orchidaceae). *Plant Systematics and Evolution* 301:609–622.

Kowalkowska AK, Margońska HB, Kozieradzka-Kiszkurno M, Bohdanowicz J. 2012. Studies on the ultrastructure of a three-spurred *fumeauxiana* form of *Anacamptis pyramidalis*. *Plant Systematics and Evolution* 298:1025–1035.

Levin E, McCue MD, Davidowitz G. 2017. More than just sugar: allocation of nectar amino acids and fatty acids in a Lepidopteran. *Proceedings of the Royal Society B: Biological Sciences* 284(1848):20162126.

Lohmann LG, Taylor CM. 2014. A new generic classification of tribe Bignonieae (Bignoniaceae). *Annals of the Missouri Botanical Garden* 99:348–489.

Lois-Milevicich J, Schilman PE, Josens R. 2021. Viscosity as a key factor in decision making of nectar feeding ants. *Journal of Insect Physiology* 128:104164.

Machado SR, de Deus Bento KB, Canaveze Y, Rodrigues TM. 2023. Peltate trichomes in the dormant shoot apex of *Metrodorea nigra*, a Rutaceae species with rhythmic growth. *Plant Biology* 25:161–175.

Machado SR, Rodrigues TM. 2021. Apoplasmic barrier in the extrafloral nectary of *Citharexylum myrianthum* (Verbenaceae). *Planta* 254:1–15.

Machado SR, Souza CVD, Guimarães E. 2016. A reduced, yet functional, nectary disk integrates a complex system of floral nectar secretion in the genus *Zeyheria* (Bignoniaceae). *Acta Botanica Brasilica* 31:344–357.

Machado SR, Canaveze Y, Rodrigues TM. 2017. Structure and functioning of oil cavities in the shoot apex of *Metrodorea nigra* A. St.-Hil. (Rutaceae). *Protoplasma* 254:1661–1674.

Mazia D, Brewer PA, Alfert M. 1953. The cytochemical staining and measurement of protein with mercuric bromphenol blue. *The Biological Bulletin* 104:57–67.

McPeek SJ, Bronstein JL, McPeek MA. 2021. The evolution of resource provisioning in pollination mutualisms. *The American Naturalist* 198(4):441–459.

Miranda P, Ribeiro JELS, Aguirre-Jaimes A, Brasil I, Dáttilo W. 2024. Morphological characterization of extrafloral nectaries in Brazilian Amazonian plant species. *Acta Botánica Mexicana* (131).

Mogensen AL, Andersen LB, Sørensen JG, Offenberg J. 2024. Manipulated ants: inducing loyalty to sugar feeders with an alkaloid. *Pest Management Science* 80(7):3445–3450.

Naczk AM, Kowalkowska AK, Wiśniewska N, Haliński ŁP, Kapusta M, Czerwicka M. 2018. Floral anatomy, ultrastructure and chemical analysis in *Dactylorhiza incarnata/maculata* complex (Orchidaceae). *Botanical Journal of the Linnean Society* 187:512–536.

Nelson AS, Acosta NC, Mooney KA. 2019. Plant chemical mediation of ant behavior. *Current Opinion in Insect Science* 32:98–103.

Nepi M, Grasso DA, Mancuso S. 2018. Nectar in plant–insect mutualistic relationships: from food reward to partner manipulation. *Frontiers in Plant Science* 9:1063.

Nepi M. 2007. Nectary structure and ultrastructure. In: Nicolson SW, Nepi M, Pacini E, eds. *Nectaries and nectar*. Dordrecht: Springer, 129–166.

Nepi M. 2017. New perspectives in nectar evolution and ecology: simple alimentary reward or a complex multiorganism interaction? *Acta Agrobotanica* 70:1.

Nepi M, Soligo C, Nocentini D, Abate M, Guarnieri M, Cai G, et al. 2012. Amino acids and protein profile in floral nectar: much more than a simple reward. *Flora – Morphology, Distribution, Functional Ecology of Plants* 207(7):475–481.

Nicolson SW. 2007. Nectar consumers. In: Nicolson SW, Nepi M, Pacini E, eds. *Nectaries and nectar*. Dordrecht: Springer, 289–342.

Nicolson SW. 2009. Water homeostasis in bees, with the emphasis on sociality. *Journal of Experimental Biology* 212(3):429–434.

Nicolson SW. 2022. Sweet solutions: nectar chemistry and quality. *Philosophical Transactions of the Royal Society B* 377:20210163.

Nogueira A, El Ottra JHL, Guimarães E, Machado SR, Lohmann LG. 2013. Trichome structure and evolution in Neotropical lianas. *Annals of Botany* 112:1331–1350.

O'Brien TP, Feder NME, McCully ME. 1964. Polychromatic staining of plant cell walls by toluidine blue O. *Protoplasma* 59:368–373.

Pacini E, Nepi M, Vesprini JL. 2003. Nectar biodiversity: a short review. *Plant Systematics and Evolution* 238:7–21.

Paiva EAS. 2016. How do secretory products cross the plant cell wall to be released? A new hypothesis involving cyclic mechanical actions of the protoplast. *Annals of Botany* 117(4):533–540.

Paiva EAS. 2017. How does the nectar of stomata-free nectaries cross the cuticle? *Acta Botanica Brasilica* 31(3):525–530.

Paiva EAS, Machado SR. 2008. The floral nectary of *Hymenaea stigonocarpa* (Fabaceae, Caesalpinioideae): structural aspects during floral development. *Annals of Botany* 101(1):125–133.

Pazouki L, Niinemets Ü. 2016. Multi-substrate terpene synthases: their occurrence and physiological significance. *Frontiers in Plant Science* 7:1019.

Petanidou T, Goethals V, Smets E. 2000. Nectary structure of Labiatae in relation to their nectar secretion and characteristics in a Mediterranean shrub community – Does flowering time matter? *Plant Systematics and Evolution* 225:103–118.

Phukela B, Adit A, Tandon R. 2020. A snapshot of evolutionary history of floral nectaries across angiosperm lineages. In: Tandon R, Shivanna K, Koul M, eds. *Reproductive Ecology of Flowering Plants: Patterns and Processes*. Singapore: Springer.

Pool A. 2009. A review of the genus *Distictella* (Bignoniaceae). *Annals of the Missouri Botanical Garden* 96(2):286–323.

Possobom CCF, Guimarães E, Machado SR. 2010. Leaf glands act as nectaries in *Diplopterys pubipetala* (Malpighiaceae). *Plant Biology* 12:863–870.

Pridgeon AM, Stern WL. 1985. Osmophores of *Scaphosepalum* (Orchidaceae). *Botanical Gazette* 146(1):115–123.

Pyke GH. 1991. What does it cost a plant to produce floral nectar? *Nature* 350:58–59.

Reinecke M, Walther C. 1978. Aspects of turnover and biogenesis of synaptic vesicles at locust neuromuscular junctions as revealed by iodide-osmium tetroxide (ZIO) reacting with intravesicular SH-groups. *Journal of Cell Biology* 21:839–855.

Reynolds ES. 1963. The use of lead citrate at high pH as an electron-opaque stain in electron microscopy. *Journal of Cell Biology* 17:208–214.

Rivera GL. 2000a. Nuptial nectary structure of Bignoniaceae from Argentina. *Darwiniana* 227–239.

Rivera GL. 2000b. Nectarios extranupciales florales en especies de Bignoniaceae de Argentina. *Darwiniana* 1–10.Roubik DW, Yanega D, Buchmann SL, Inouye DW. 1995. On optimal nectar foraging by some tropical bees (Hymenoptera: Apidae). *Apidologie* 26(3):197–211.

Sá-Haiad B, Silva CP, Paula RCV, Rocha JF, Machado SR. 2015. Androecia in two *Clusia* species: development, structure and resin secretion. *Plant Biology* 17(4):816–824.

Schmitt A, Roy R, Carter CJ. 2021. Nectar antimicrobial compounds and their potential effects on pollinators. *Current Opinion in Insect Science* 44:55–63.

Seibert RJ. 1948. The use of glands in a taxonomic consideration of the family Bignoniaceae. *Annals of the Missouri Botanical Garden* 35(2):123–137.

Slavković F, Bendahmane A. 2023. Floral phytochemistry: impact of volatile organic compounds and nectar secondary metabolites on pollinator behavior and health. *Chemistry & Biodiversity* 20(4):e202201139.

Southwick EE. 1984. Photosynthate allocation to floral nectar: a neglected energy investment. *Ecology* 65(6):1775–1779.

Stern WL, Curry KJ, Pridgeon AM. 1987. Osmophores of *Stanhopea* (Orchidaceae). *American Journal of Botany* 74(9):1323–1331.

Stone TB, Thompson AC, Pitre HN. 1985. Analysis of lipids in cotton extrafloral nectar. *Journal of Entomological Science* 20(4):422–428.

Stpiczyńska M, Davies KL, Gregg A. 2005. Comparative account of nectary structure in *Hexisea imbricata* (Lindl.) Rchb. f. (Orchidaceae). *Annals of Botany* 95(5):749–756.

Stpiczyńska M, Davies KL. 2016. Evidence for the dual role of floral secretory cells in *Bulbophyllum*. *Acta Biologica Cracoviensia. Series Botanica* 58(2).

Stpiczyńska M, Kamińska M, Davies KL. 2021. Nectar secretion in a dry habitat: structure of the nectary in two endangered Mexican species of *Barkeria* (Orchidaceae). *PeerJ* 9:e11874.

Subramanian RB, Inamdar JA. 1985. Occurrence, structure, ontogeny and biology of nectaries in *Kigelia pinnata* DC. *The Botanical Magazine: Shokubutsu-gaku-zasshi* 98:67–73.

Suissa JS, Li FW, Moreau CS. 2024. Convergent evolution of fern nectaries facilitated independent recruitment of ant-bodyguards from flowering plants. *Nature Communications* 15(1):4392.

Taiz L, Zeiger E, Møller IM, Murphy A. 2013. *Plant Physiology and Development*. 6th edn. Sunderland: Sinauer Associates.

Thomas V, Dave Y. 1992. Structure and biology of nectaries in *Tabebuia serratifolia* Nichols (Bignoniaceae). *Botanical Journal of the Linnean Society* 109(3):395–400.

Tölke EED, Galetto L, Machado SR, Lacchia APS, Carmello-Guerreiro SM. 2015. Stages of development of the floral secretory disk in *Tapirira guianensis* Aubl. (Anacardiaceae), a dioecious species. *Botanical Journal of the Linnean Society* 179(3):533–544.

Vaudo AD, Tooker JF, Grozinger CM, Patch HM. 2015. Bee nutrition and floral resource restoration. *Current Opinion in Insect Science* 10:133–141.

Weber MG, Keeler KH. 2013. The phylogenetic distribution of extrafloral nectaries in plants. *Annals of Botany* 111(6):1251–1261.

Wiśniewska N, Kowalkowska AK, Kozieradzka-Kiszkurno M, Krawczyńska AT, Bohdanowicz J. 2018. Floral features of two species of *Bulbophyllum* section *Lepidorhiza* Schltr.: *B. levanae* Ames and *B. nymphopolitanum* Kraenzl. (Bulbophyllinae Schltr., Orchidaceae). *Protoplasma* 255:485–499.

Wist TJ, Davis AR. 2006. Floral nectar production and nectary anatomy and ultrastructure of *Echinacea purpurea* (Asteraceae). *Annals of Botany* 97(2):177–193.

Yanagizawa Y, Gottsberger G. 1982. Competition between *Distictella elongata* (Bignoniaceae) and *Crotalaria anagyroides* (Fabaceae) in relation to pollinating bees on the cerrado of Botucatu, São Paulo State, Brazil. *[journal name not specified]*

Zhou Y, Ding S, Liao C, Wu J, Chittka L, Solvi C, Peng F. 2024. Bumble bees' food preferences are jointly shaped by rapid evaluation of nectar sugar concentration and viscosity. *Animal Behaviour* 210:419–427.

Pais MS, Figueiredo ACS. 1994. Floral nectaries from *Limodorum abortivum* (L) Sw and *Epipactis atropurpurea* Rafin (Orchidaceae): ultrastructural changes in plastids during the secretory process. *Apidologie 25*(6): 615-626.

Xun L, Huang R, Li Q, Meng Q, Su R, Wu X, Zhang R, Li L, Gong X, Dong K. 2025. Specialized metabolites present in *Camellia reticulata* nectar inhibit the growth of nectar-inhabiting microorganisms. *Frontiers in Plant Science*, 16: 1557228.

## Figure legends

**Figure 1**. Inflorescence and flowers of *Amphilophium mansoanum* (Bignoniaceae). (A) Inflorescence with flowers in different developmental stages. Note ants on the calyx margin in the pre-anthesis bud. (B) Clustered prominent pores arranged in longitudinal bands at the distal region of the young bud. (C) Pre-anthesis bud sectioned longitudinally in the median plane showing a nectary at the base of the ovary and nectariferous chamber. (D) Extranuptial nectar droplets at the calyx margin of the young and pre-anthesis buds.

**ALT TEXT:** Photographs labelled A to D. A shows an inflorescence with flowers in different developmental stages with ants on the calyx margin in the pre-anthesis bud. B shows clustered prominent pores arranged in longitudinal bands at the distal region of the young bud. C shows a pre-anthesis bud sectioned longitudinally in the median plane showing a nectary at the base of the ovary and nectariferous chamber. D shows extranuptial nectar droplets at the calyx margin of the young and pre-anthesis buds.

**Figure 2**. Micrographs of the nuptial nectary of *Amphilophium mansoanum* (Bignoniaceae) (A) Appearance of the nectary disk in pre-anthesis buds seen under a stereomicroscope. (B-F) SEM micrographs. (B) Stomata irregularly distributed on the nectary disk surface. (C) Detail showing ordinary stomata together with prominent large stomata with wide pores. Note the guard cells with cuticular ledges. (D) Giant raised stoma. (E) First day flower; nectary disk covered with flocculant secretion residues. (F) Raised stoma with wide circular pore filled with secretion residues.

**ALT TEXT:** Micrographs of the nuptial nectary of *Amphilophium mansoanum* labelled A to F. A shows the nectary disk in pre-anthesis buds seen under a stereomicroscope. B-F are SEM micrographs. B shows stomata irregularly distributed on the nectary disk surface. C shows ordinary stomata together with prominent large stomata with wide pores, which guard cells have cuticular ledges. D shows giant raised stoma. E shows the nectary disk of a first day flower covered with flocculant secretion residues. F shows raised stoma with wide circular pore filled with secretion residues.

**Figure 3**. Light micrographs of cross-sections of the nuptial nectary of *Amphilophium mansoanum* (Bignoniaceae). (A-F) Pre-anthesis buds. (A) General view of the nectary with epidermis, nectary parenchyma underneath the epidermis, and subnectary parenchyma. (B) Detail showing scarce starch grains in the parenchyma. (C) Vascular bundles in the subnectary parenchyma. Note predominance of phloem. (D) Abundance of starch grains in the subnectary parenchyma. (E) Intercellular spaces filled with secretions in the nectary parenchyma. (F) Stoma with a wide opening. (G-J) First-day flowers. (G)

Nectary parenchyma showing rounded cells with large vacuole and dense accumulations. (H) Subnectary parenchyma with vacuolated cells. (I) Parenchyma cells with phenolic compounds and sparse voluminous starch grains. (J) Tracheary elements in the subnectary parenchyma. Key to figures: ep, epidermis; ie, intercellular space; np, nectary parenchyma; sp, subnectary parenchyma; vb, vascular bundles; xy, xylem.

**ALT TEXT:** Light micrographs of cross-sections of the nuptial nectary of *Amphilophium mansoanum* labelled A to J. A-F show light micrographs of pre-anthesis buds. A shows a general view of the nectary with epidermis, nectary parenchyma underneath the epidermis, and subnectary parenchyma. B shows scarce starch grains in the parenchyma. C shows vascular bundles in the subnectary parenchyma with predominance of phloem. D shows abundance of starch grains in the subnectary parenchyma. E shows intercellular spaces filled with secretions in the nectary parenchyma. F shows a stoma with a wide opening. G-J show light micrographs of first-day flowers. G shows nectary parenchyma presenting rounded cells with large vacuole and dense accumulations. H shows subnectary parenchyma with vacuolated cells. I shows parenchyma cells with phenolic compounds and sparse voluminous starch grains. J shows tracheary elements in the subnectary parenchyma.

**Figure 4.** Histochemical characterization of the nuptial nectary of *Amphilophium mansoanum* (Bignoniaceae); cross-sections. (A-B) Positive reaction to test with mercury blue bromophenol reagent, evidencing the presence of basic proteins in the vascular bundles (vb), and in the parenchyma cells (arrowhead). (C) Positive reaction to test with Alcian Blue, evidencing the presence of acid polysaccharides. (D) Positive reaction to the test with NADI reagent (arrowhead), evidencing the presence of essential oils (blue staining) and oils-resin (pink staining). (E) Positive reaction to test with Lugol reagent (arrowhead), evidencing the presence of starch grains. (F-G) Positive reaction to test with Sudan IV (arrowhead), evidencing the presence of lipids. (H) Positive reaction to test with ferric chloride reagent (arrowhead), evidencing the presence of phenolic compounds.

**ALT TEXT:** Histochemical characterization of cross sections of the nuptial nectary of *Amphilophium mansoanum* labelled A to H. A-B show positive reaction to test with mercury blue bromophenol reagent, evidencing the presence of basic proteins in the vascular bundles (vb), and in the parenchyma cells (arrowhead). C shows positive reaction to test with Alcian Blue, evidencing the presence of acid polysaccharides. D shows positive reaction to the test with NADI reagent (arrowhead), evidencing the presence of essential oils (blue staining) and oils-resin (pink staining). E shows positive reaction to test with Lugol reagent (arrowhead), evidencing the presence of starch grains. F-G show positive reaction to

test with Sudan IV (arrowhead), evidencing the presence of lipids. H shows positive reaction to test with ferric chloride reagent (arrowhead), evidencing the presence of phenolic compounds.

**Figure 5**. Transmission electron micrographs of the nuptial nectary of *Amphilophium mansoanum* in pre-anthesis buds. (A-C) Epidermal cells. (A) Part of an epidermal cell with thick outer periclinal wall and thin cuticle, abundant cytoplasm, endoplasmic reticulum, starch grains and oil drops. Note the osmiophilic body in the periplasmic space (arrow). (B) Endoplasmic reticulum profiles at the peripheral cytoplasm, dictyosomes and vesicles marked by ZIO method, rounded leucoplast with a large osmiophilic inclusion, and ellipsoid amyloplast. Note electron dense granules in the periplasmic space and attached to the tonoplast. (C) Abundant vesicles from dictyosomes filled with dense content marked by ZIO method, and dense material inside the vacuole. Note the lipid drop at the peripheral cytoplasm. (D-F) Nectary parenchyma. (D) Parenchyma cells with very thin walls (arrowhead), nucleus and large vacuoles filled with flocculant materials. (E) Starch grains with different sizes and degradation signals. (F) Plastids with starch grains and osmiophilic globules. Note osmophilic bodies attached to the tonoplast. (G-I) Subnectary parenchyma. (G) Phloem and vacuolated parenchyma cells with big amyloplasts. (H) Plasmodesmata in the transversal walls connecting parenchyma cells (arrow heads). (I) Parenchyma cells with conspicuous nucleus, abundant cytoplasm, big amyloplasts and vacuoles with flocculent materials. Note the intercellular spaces with fibrillar materials. (J-L) Phloem in the subnectary parenchyma. (J) Several phloem cells in the subnectary parenchyma. (K) Sieve tube elements of large caliber. (L) Phloem cells with voluminous amyloplasts with intact starch grains. Key to figures: am, amyloplast; cc, companion cell; ct, cuticle; cw, cell wall; is, intercellular space; le, leucoplast; nu, nucleus; ol, oil drop; pe, periplasmic space; pp, phloem parenchyma; pl, plastid; sg, starch grain; sp, subnectary parenchyma; ste, sieve tube element; va, vacuole.

**ALT TEXT:** Transmission electron micrographs of the nuptial nectary of *Amphilophium mansoanum* in pre-anthesis buds labelled A to L. A-C TEM micrographs show epidermal cells. A shows part of an epidermal cell with thick outer periclinal wall and thin cuticle, abundant cytoplasm, endoplasmic reticulum, starch grains, oil drops and osmiophilic body in the periplasmic space (arrow). B shows endoplasmic reticulum profiles at the peripheral cytoplasm, dictyosomes and vesicles marked by ZIO method, rounded leucoplast with a large osmiophilic inclusion, ellipsoid amyloplast and dense granules in the periplasmic space and attached to the tonoplast. C shows abundant vesicles from dictyosomes filled with dense content marked by ZIO method, dense material inside the vacuole, and a lipid drop at the peripheral cytoplasm. D-F TEM micrographs show nectary parenchyma. D shows parenchyma cells with very thin walls (arrowhead), nucleus and large vacuoles filled with flocculant materials. E shows

starch grains with different sizes and degradation signals. F shows plastids with starch grains and osmiophilic globules, and osmophilic bodies attached to the tonoplast. G-I TEM micrographs show subnectary parenchyma. G shows phloem and vacuolated parenchyma cells with big amyloplasts. H shows plasmodesmata in the transversal walls connecting parenchyma cells (arrow heads). I shows parenchyma cells with conspicuous nucleus, abundant cytoplasm, big amyloplasts and vacuoles with flocculent materials, and intercellular spaces with fibrillar materials. J-L TEM micrographs show phloem in the subnectary parenchyma. J shows several phloem cells in the subnectary parenchyma. K shows sieve tube elements of large caliber. L shows phloem cells with voluminous amyloplasts with intact starch grains

**Figure 6**. Transmission electron micrographs of the nuptial nectary of *Amphilophium mansoanum* (Bignoniaceae). (A-I) First-day flowers; (J-N) Second-day flowers. (A-C) Epidermal cells. (A) Large vacuole in the apical pole and clustered dense plastids with small starch grains in the basal pole. (B) Granulated cytoplasm with scattered oil drops, and vacuoles with flocculant material. Note the periplasmic space along the outer cell wall. (C) Secretion residues (arrow) on the cuticle. Note microchannels projecting from the cell wall to the cuticle. (D) Nectary parenchyma cell with collapsed amyloplasts and broken starch grains. (E) Subnectary parenchyma with vacuoles full of fibrillar or flocculant materials, membrane debris, and osmiophilic inclusions. Note larger intercellular spaces filled with fibrillar material. (F-I) Phloem features in the subnectary parenchyma. (F) Vacuolated parenchyma cell containing broken starch grains. (G) Sieve plate plugged with amorphous deposits, typically callose. (H) Parenchyma cell with spindle-shaped protein bodies scattered in the cytoplasm. (I) Parenchyma cell showing dictyosomes and vesicles marked by ZIO reaction. (J) Epidermal cells with reduced cytoplasm and big vacuoles with fibrillar inclusion and membrane debris. Note denser clustered plastids with tiny starch grains. (K) Nectary parenchyma showing vacuolated cells with reduced cytoplasm, and intercellular spaces. (L) Subnectary parenchyma with wider intercellular spaces; cells showing nucleus, reduced cytoplasm and big amyloplasts. Note dark inclusion in the vacuole. (M) Detail showing part of the nucleus, endoplasmic reticulum element, mitochondria, amyloplast containing one starch grain and osmiophilic bodies, and vacuole. (N) Detail of the subnectary parenchyma showing intercellular space filled with fibrillar material. Note dark inclusion in the vacuole (arrow). Key to figures: ct, cuticle; cw, cell wall; di, dictyosome; er, endoplasmic reticulum; ie, intercellular space; mi, mitochondria; nu, nucleus; ol, oil drop; pb, protein bodies; pp, phloem parenchyma; pl, plastid; ste, sieve tube element; va, vacuole.

**ALT TEXT:** Transmission electron micrographs of the nuptial nectary of *Amphilophium mansoanum* labelled A to N. A-I TEM micrographs show first-day flowers; J-N TEM micrographs show second-day flowers. A-C show epidermal cells. A shows large vacuole in the apical pole and clustered dense plastids with small starch grains in the basal pole. B shows granulated cytoplasm with scattered oil drops, vacuoles with flocculant material, and periplasmic space along the outer cell wall. C shows secretion residues (arrow) on the cuticle, and microchannels projecting from the cell wall to the cuticle. D shows nectary parenchyma cell with collapsed amyloplasts and broken starch grains. E shows subnectary parenchyma with vacuoles full of fibrillar or flocculant materials, membrane debris, osmiophilic inclusions, and larger intercellular spaces filled with fibrillar material. F-I TEM micrographs show phloem features in the subnectary parenchyma. F shows vacuolated parenchyma cell containing broken starch grains. G shows sieve plate plugged with amorphous deposits, typically callose. H shows parenchyma cell with spindle-shaped protein bodies scattered in the cytoplasm. I shows parenchyma cell showing dictyosomes and vesicles marked by ZIO reaction. J shows epidermal cells with reduced cytoplasm and big vacuoles with fibrillar inclusion and membrane debris, and denser clustered plastids with tiny starch grains. K shows nectary parenchyma showing vacuolated cells with reduced cytoplasm and intercellular spaces. L shows subnectary parenchyma with wider intercellular spaces; cells showing nucleus, reduced cytoplasm, big amyloplasts, and dark inclusion in the vacuole. M details part of the nucleus, endoplasmic reticulum element, mitochondria, amyloplast containing one starch grain and osmiophilic bodies, and vacuole. N details the subnectary parenchyma showing intercellular space filled with fibrillar material, and dark inclusion in the vacuole (arrow).

**Figure 7**. Extranuptial nectary of *Amphilophium mansoanum* (Bignoniaceae). (A-D) Scanning electron micrographs of the calyx surface. (A) Clustered concave glands at the surface of young flower buds surrounded by trichomes. (B) Gland with extended margin that projects above the surface of the calyx forming a wide central cavity. (C) Non-glandular trichomes, peltate glandular trichome, and raised stomata (arrow). (D) Gland sectioned longitudinally showing the concave portion located above the calyx surface and the portion immersed in the calyx mesophyll. (E-J) Light micrographs of the transversal section, stained with toluidine blue, showing glands at different developmental stages. (E-G) 6 µm thick; (H-J) 60 nm thick. (E-F) Young bud. (E) Gland formed by secretory head with undeveloped margin, uniseriate stalk, and parenchyma foot. (F) Detail showing head cells covered with a thick cuticle, and stalk cells with thick lateral walls. (G) Small subcuticular space in the central region of the secretory head with secretion accumulation (arrow). (H) Pre-anthesis bud; head secretory cells and foot cells with strongly stained dense cytoplasm. (I) First-day flowers; gland with expanded margin perpendicular to the

surface of the calyx. Note that all gland cells have less dense content and more developed vacuoles. (J) Detrail showing ticker cuticle, head cells with thick walls, prominent nucleus and vacuoles with different sizes. Note the thick-walled stalk cells and dense granulations in the foot cells. Key to figures: pg, patelliform-gland; pt, peltate glandular trichome; nt, non-glandular trichome; sh, secretory head; st, stalk; ft, foot.

**ALT TEXT:** Extranuptial nectary of *Amphilophium mansoanum* labelled A to J. A-D shows scanning electron micrographs of the calyx surface. A shows clustered concave glands at the surface of young flower buds surrounded by trichomes. B shows gland with extended margin that projects above the surface of the calyx forming a wide central cavity. C shows non-glandular trichomes, peltate glandular trichome, and raised stomata (arrow). D shows gland sectioned longitudinally showing the concave portion located above the calyx surface and the portion immersed in the calyx mesophyll. E-J show light micrographs of the transversal section, stained with toluidine blue, showing glands at different developmental stages. E-F shows a young bud. E shows gland formed by secretory head with undeveloped margin, uniseriate stalk, and parenchyma foot. F details head cells covered with a thick cuticle, and stalk cells with thick lateral walls. G shows small subcuticular space in the central region of the secretory head with secretion accumulation (arrow). H shows pre-anthesis bud; head secretory cells and foot cells with strongly stained dense cytoplasm. I shows first-day flowers; gland with expanded margin perpendicular to the surface of the calyx. All gland cells have less dense content and more developed vacuoles. J details ticker cuticle, head cells with thick walls, prominent nucleus, vacuoles with different sizes, thick-walled stalk cells and dense granulations in the foot cells.

**Figure 8**. Histochemical characterization of the extranuptial nectary of *Amphilophium mansoanum* (Bignoniaceae); cross-sections. (A-B) Positive reaction to starch grains and to alkaloids with Lugol. (A) Note the vascular bundles in the calyx mesophyll (arrowhead) ending at the foot of the gland. (B) Positive reaction more evident in the foot cells underlying the gland stalk and in the upper region of the secretory head. (C-E) Positive reaction to test with Sudan IV. (C) Presence of lipids in the lateral walls of the stalk cells and cuticle. (D) Lipid droplets (arrowhead) in the head cells. (E) Lipid droplets (arrowhead) in the foot cells. (F) Positive reaction to test with mercury blue bromophenol reagent, evidencing the presence of basic proteins in the head cells. (G) Positive reaction to test with NADI reagent (arrowhead), evidencing the presence of oils-resin (pink staining) in the head cells. (H) Positive reaction to test with ferric chloride reagent, evidencing the presence of alkaloids (stained reddish brown) in the foot cells. (I) Positive reaction to ruthenium red test, evidencing the presence of pectin in the cell walls of the central

region of the secretory head and in the foot of the gland. Key to figures: ft, foot; sh, secretory head; st, stalk.

**ALT TEXT:** Histochemical characterization of the extranuptial nectary of *Amphilophium mansoanum* labelled A to I. A-B show positive reaction to starch grains and to alkaloids with Lugol. A shows the vascular bundles in the calyx mesophyll (arrowhead) ending at the foot of the gland. B shows positive reaction more evident in the foot cells underlying the gland stalk and in the upper region of the secretory head. C-E show positive reaction to test with Sudan IV. C shows presence of lipids in the lateral walls of the stalk cells and cuticle. D shows lipid droplets (arrowhead) in the head cells. E shows lipid droplets (arrowhead) in the foot cells. F shows positive reaction to test with mercury blue bromophenol reagent, evidencing the presence of basic proteins in the head cells. G shows positive reaction to test with NADI reagent (arrowhead), evidencing the presence of oils-resin (pink staining) in the head cells. H shows positive reaction to test with ferric chloride reagent, evidencing the presence of alkaloids (stained reddish brown) in the foot cells. I shows positive reaction to ruthenium red test, evidencing the presence of pectin in the cell walls of the central region of the secretory head and in the foot of the gland.

**Figure 9.** Transmission electron micrographs of the extranuptial nectary of *Amphilophium mansoanum* (Bignoniaceae). (A-C) Glands in young buds; (D-I) Glands in pre-anthesis buds. (A) Head cells with spherical and organized nucleolus, dense cytoplasm, and poorly developed vacuoles. (B) Amyloplasts with lots of starch grains, mitochondria, and small vacuole. (C) Amyloplasts, mitochondria, and dictyosomes with adjacent vesicles containing electron-dense material, marked by ZIO. (D) Mitochondria and extensive endoplasmic reticulum profiles. (E) Plastid with residual starch grains and a big osmiophilic inclusion. Note the endoplasmic reticulum around the plastid, and the plasmodesmata in the anticlinal walls of the head cells. (F) Elongated leucoplast devoid of inner membranes with homogeneous stroma surrounded by endoplasmic reticulum. (G) Dictyosomes and vesicles, marked by ZIO reaction, and endoplasmic reticulum profiles close to plasmodesmata (arrowhead). Note the dense materials close to the plasma membrane and in the periplasmic space (arrows). (H) Stalk cell with thin anticlinal walls and thickened lateral walls showing central nucleus and endoplasmic reticulum. (I) Gland foot formed by tangentially expanded cells with dense inclusions in the vacuoles. Note cytoplasmic oil body. Key to figures: cw, cell wall; di, dictyosome; er, endoplasmic reticulum; is, intercellular space; le, leucoplast; mi, mitochondria; nu, nucleus; ol, oil body; pl, plastid; sg, starch grain; sh, secretory head; st, stalk; va, vacuole.

**ALT TEXT:** Transmission electron micrographs of the nuptial nectary of *Amphilophium mansoanum* labelled A to I. A-C shows glands in young buds; D-I shows glands in pre-anthesis buds. A shows head

cells with spherical and organized nucleolus, dense cytoplasm, and poorly developed vacuoles. B shows amyloplasts with lots of starch grains, mitochondria, and small vacuole. C shows amyloplasts, mitochondria, and dictyosomes with adjacent vesicles containing electron-dense material, marked by ZIO. D shows mitochondria and extensive endoplasmic reticulum profiles. E shows plastid with residual starch grains and a big osmiophilic inclusion, endoplasmic reticulum around the plastid, and the plasmodesmata in the anticlinal walls of the head cells. F shows elongated leucoplast devoid of inner membranes with homogeneous stroma surrounded by endoplasmic reticulum. G shows dictyosomes and vesicles, marked by ZIO reaction, endoplasmic reticulum profiles close to plasmodesmata (arrowhead), and dense materials close to the plasma membrane and in the periplasmic space (arrows). H shows stalk cell with thin anticlinal walls and thickened lateral walls showing central nucleus and endoplasmic reticulum. I shows gland foot formed by tangentially expanded cells with dense inclusions in the vacuoles. Note cytoplasmic oil body.

**Figure 10**. Transmission electron micrographs of the extranuptial nectary of *Amphilophium mansoanum* (Bignoniaceae). (A-H) First-day flowers; (I-L) Second-day flowers. (A) General view showing thick cuticle with accumulations of electron dense material. Note the dark and clear cells with thicker walls. (B) Head cells with voluminous nucleus, abundant cytoplasm, and large lipid drops. (C) Periplasmic spaces along the anticlinal walls containing paramural bodies. (D) Lipid inclusions in the anticlinal walls of the head cells. (E) Polymorphic plastids with finely granular stroma and osmiophilic inclusions (likely terpene/phenols). (F) Stalk cell with large lipid bodies, mitochondria, and small vacuoles. (G) Gland foot with wider intercellular spaces filled with fibrillar material, and cells with prominent nucleus, abundant cytoplasm and small vacuoles with electron dense bodies. (H) Detail of a foot cell with numerous mitochondria, electron-dense plastids and small vacuoles. (I) Apical region of the head with abundant dark cells. (J) Larger accumulations of electron-dense material in the cuticle. (K) Dark cells with abundant cytoplasm, rich in intact organelles and small vacuoles. (L) Dark cell showing well-developed Golgi bodies with numerous cisternae, sparse profiles of endoplasmic reticulum, oil bodies, and vacuoles with membrane debris. Key to figures: ct, cuticle; cw, cell wall; di, dictyosome; dc, dark cells; er, endoplasmic reticulum; ie, intercellular space; mi, mitochondria; nu, nucleus; ol, oil drop; pl, plastid; ps, periplasmic space; sg, starch grain; st, stalk; va, vacuole.

**ALT TEXT:** Transmission electron micrographs of the extranuptial nectary of *Amphilophium mansoanum* labelled A to L. A-H show first-day flowers; I-L show second-day flowers. A shows aeneral view showing thick cuticle with accumulations of electron dense material, and dark and clear cells with thicker walls. B shows head cells with voluminous nucleus, abundant cytoplasm, and large lipid drops.

C shows periplasmic spaces along the anticlinal walls containing paramural bodies. D shows lipid inclusions in the anticlinal walls of the head cells. E shows polymorphic plastids with finely granular stroma and osmiophilic inclusions (likely terpene/phenols). F shows stalk cell with large lipid bodies, mitochondria, and small vacuoles. G shows gland foot with wider intercellular spaces filled with fibrillar material, and cells with prominent nucleus, abundant cytoplasm and small vacuoles with electron dense bodies. H details a foot cell with numerous mitochondria, electron-dense plastids and small vacuoles. I show apical region of the head with abundant dark cells. J shows larger accumulations of electron-dense material in the cuticle. K shows dark cells with abundant cytoplasm, rich in intact organelles and small vacuoles. L shows dark cell showing well-developed Golgi bodies with numerous cisternae, sparse profiles of endoplasmic reticulum, oil bodies, and vacuoles with membrane debris.

**Table 1.** Sites of histochemical reaction in nuptial and extranuptial nectaries of *Amphilophium mansoanum* flowers. These results are shown in Figures 4 and 8. NA, not applicable; inconclusive results; NN, nuptial nectary; ENN, extranuptial nectary; ep, epidermis; np, nectary parenchyma; snp, subnectary parenchyma; ft, foot cells; st, stalk cells; sh, secretory head; cw, cell wall; is, intercellular space; ic, intracellular; ex, extracuticular; cu, cuticle; scu, subcuticular space; vb, vascular bundles.

| Stage | Nectary type | Reagents and target compounds | | | | | | | |
|---|---|---|---|---|---|---|---|---|---|
| | | Ferric chloride (Phenolic substances) | Lugol (Starch grains) | Lugol (Alkaloids) | NADI (Terpenes) | Ruthenium red (Pectin) | Sudan (Lipids) | Alcian Blue (Acid polysaccharides) | Mercuric bromophenol blue (Proteins) |
| **Young bud** | NN | snp (ic) | snp (ic) | snp (ic) | NA | ep (na) np (cw) snp (cw) | snp (ic) | NA | NA |
| | ENN | NA | ft (ic) st (ic) sh (ic) | NA | NA | sh (ic) | st (cw) sh (cu) | NA | NA |
| **Pre-anthesis bud** | NN | ep (ic) np (ic) snp (ic) | ep snp (ic) | ep (ic) | ep (ic; ex) np (ic) snp (ic) | ep (cu; ic; cw;) np (is; cw; ic) snp (cw; vb) | ep (cu; ic) np (ic) snp (ic) | NA | NA |
| | ENN | sh (ic) ft (ic) | ft (ic) | ft (ic) | NA | ft (cw; ic), st (ic) sh (cw; ic) | ft (ic) st (cw; ic) sh (ic; cu; scu) | NA | NA |
| **First-day flower** | NN | ep (ic) np (ic) snp (ic) | ep (ic) np (ic) snp (ic) | np (ic) snp (ic) | ep (ex) np (ic) snp (ic; is) | ep (cw) np (cw) snp (cw) | ep (na) np (na) snp (is; ic) | ep (cw; ic) np (cw; ic) snp (cw; ic) | ep (ic) np (ic) snp (ic; vb) |
| | ENN | ft (ic) | ft (ic) sh (ic) | ft (ic) st (ic) sh (ic) | sh (ic) | ft (cw; is; ic) st (ic) sh (cw; ic) | st (cw) sh (cu) | sh (cw; scu) ft (is; cw) | sh (ic) |
| | NN | np (ic) snp (ic) | ep (ic) np (ic) | snp (ic) | ep (ic) np (ic) | ep (cw) np (cw; ic) | ep (cu; ic) | NA | NA |

| | | | | | | | | | |
|---|---|---|---|---|---|---|---|---|---|
| | | | snp (ic) | | snp (ic) | snp (cw; vb; ic) | np (ic) snp (ic) | | |
| **Second-day flower** | ENN | ft (ic) sh (ic) | sh (ic) ft (ic) | ft (ic) | NA | sh (ic) ft (ic; cw) | ft (ic) st (cw) sh (cu; ic) | NA | NA |

1

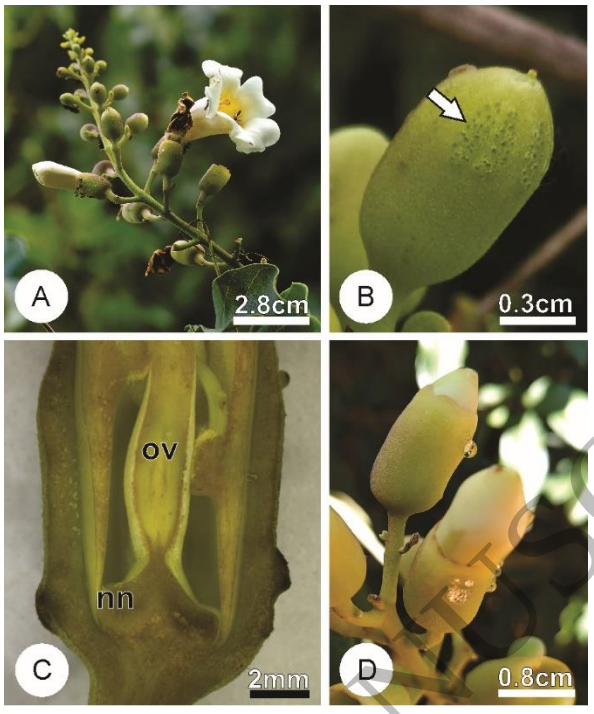


*Figure 1*
*77x93 mm ( x DPI)*

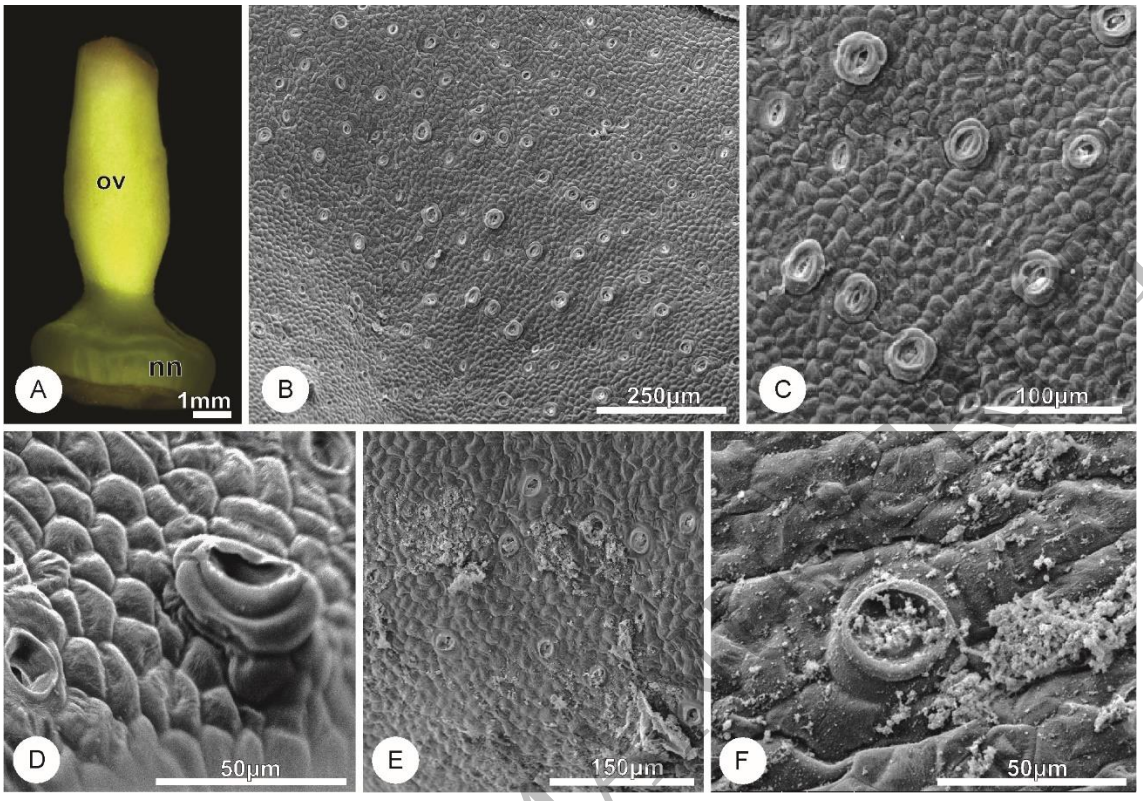


*Figure 2*
*150x104 mm ( x DPI)*

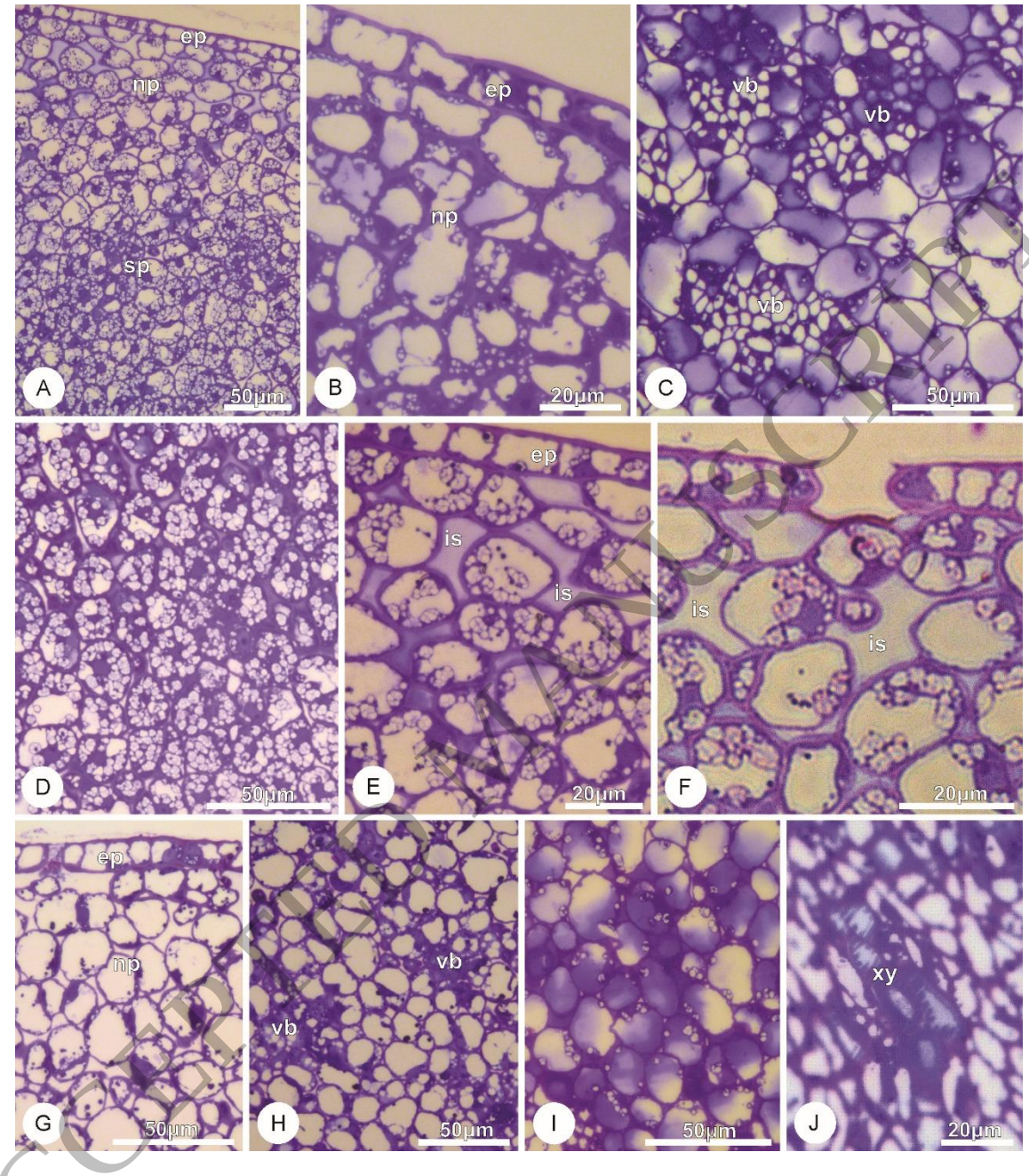


*Figure 3*
*150x171 mm ( x DPI)*

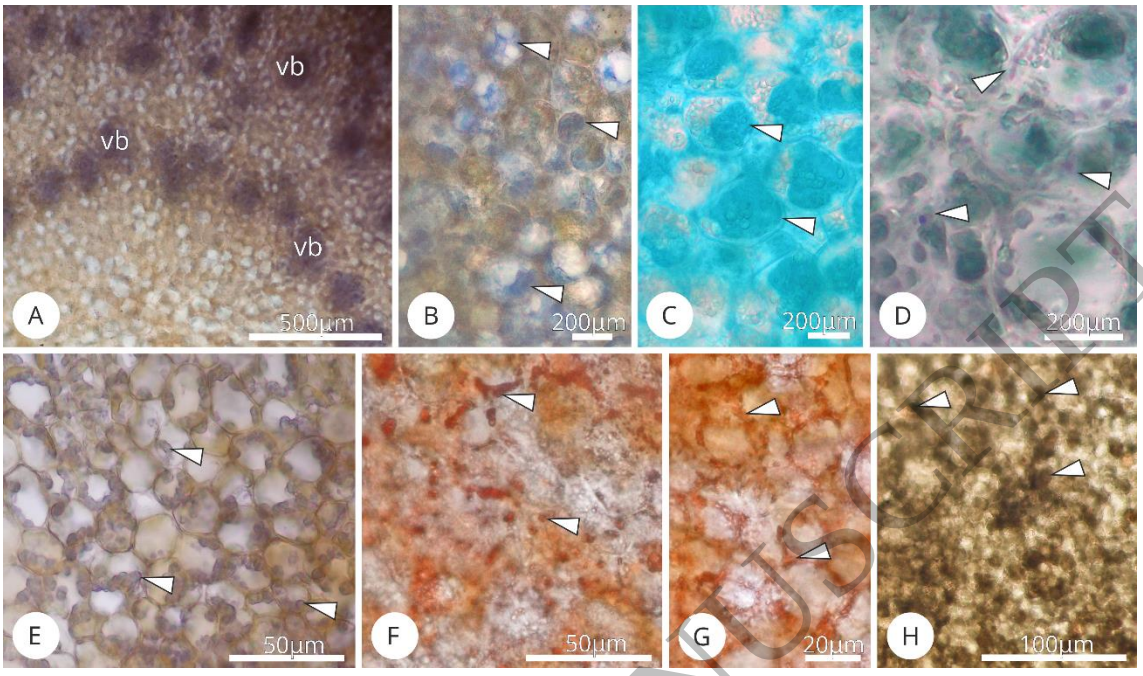


*Figure 4*
*150x88 mm ( x DPI)*

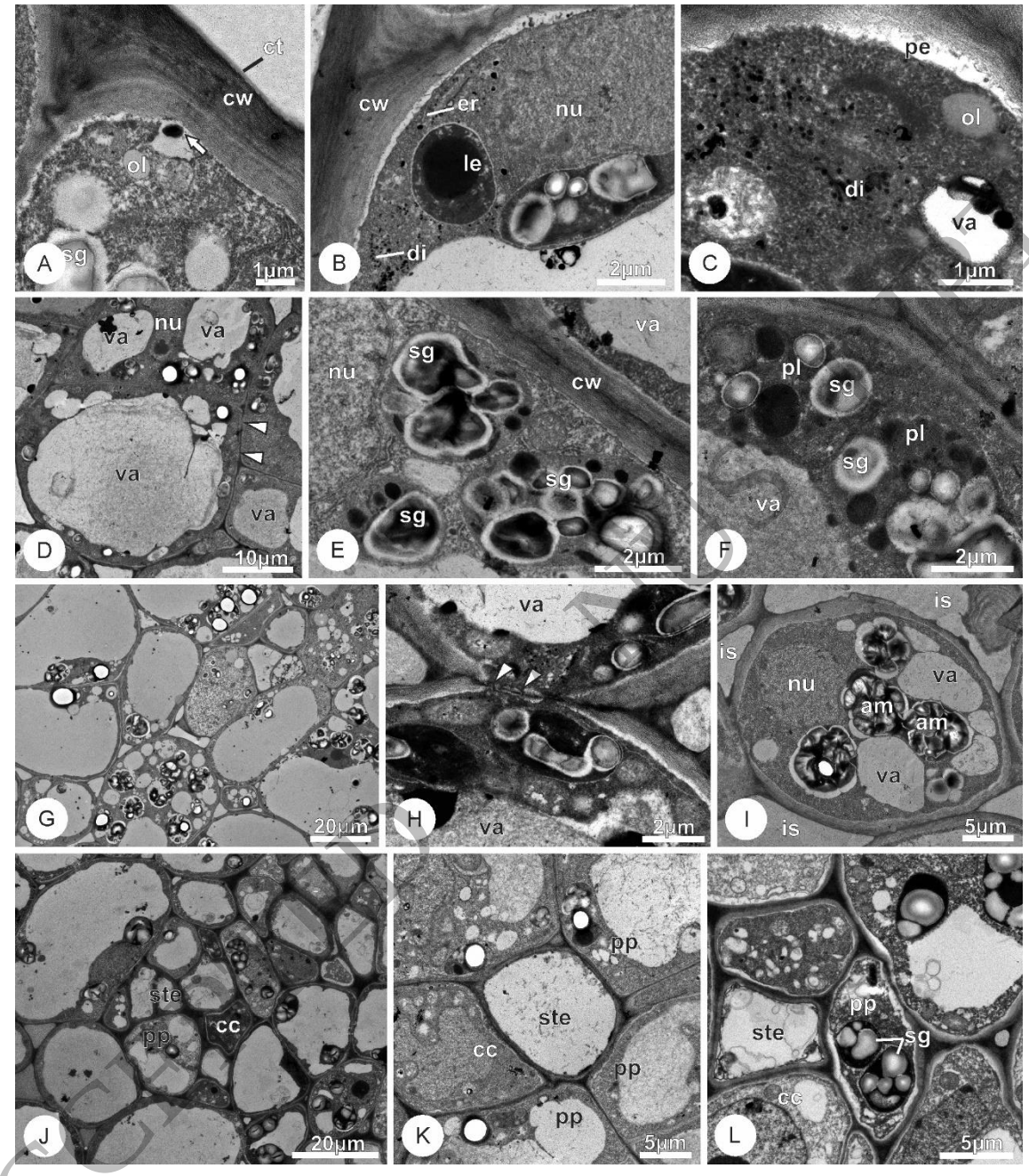


*Figure 5*
*150x173 mm ( x DPI)*

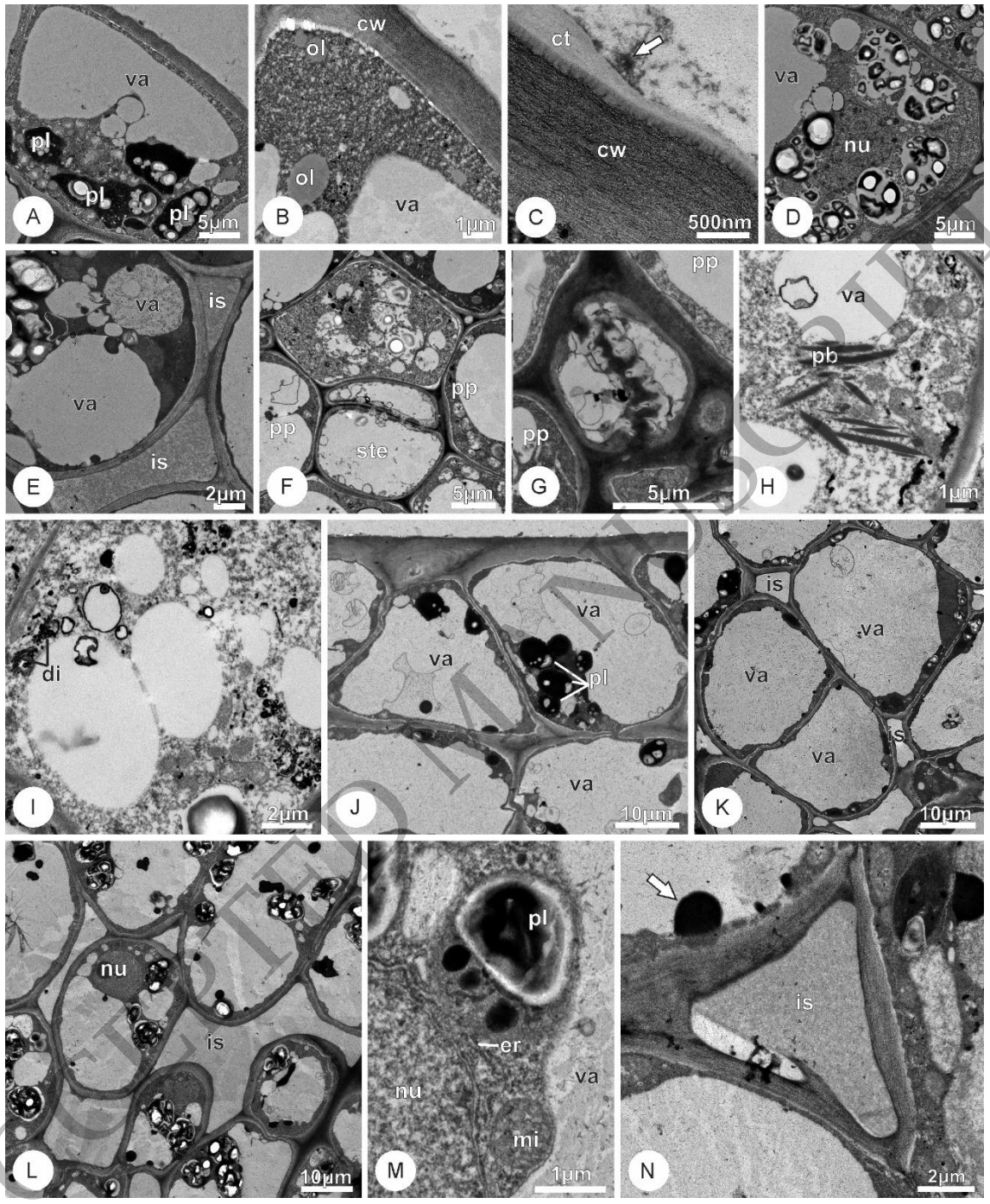


*Figure 6*
*150x183 mm ( x DPI)*

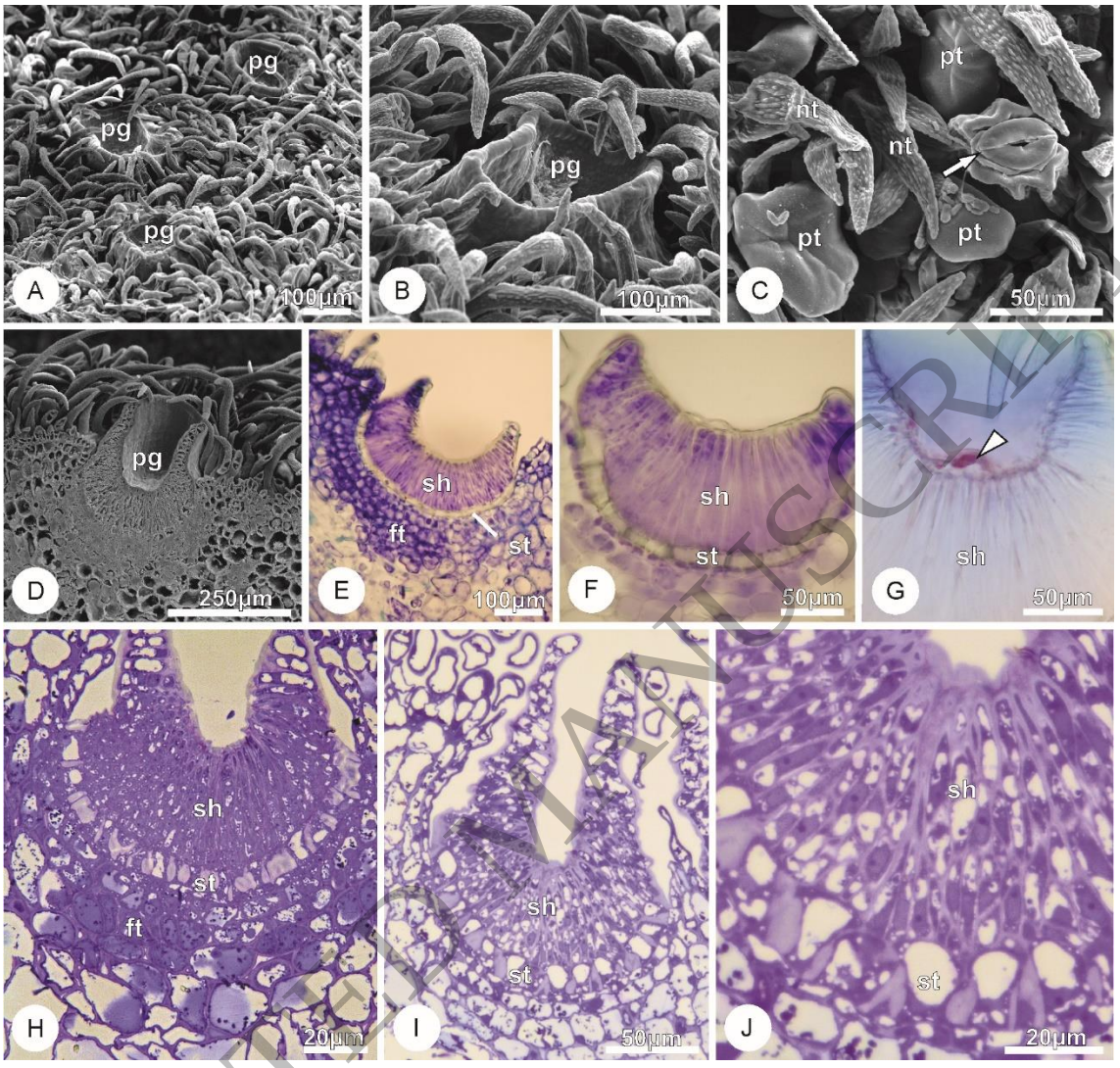


*Figure 7*
*150x143 mm ( x DPI)*

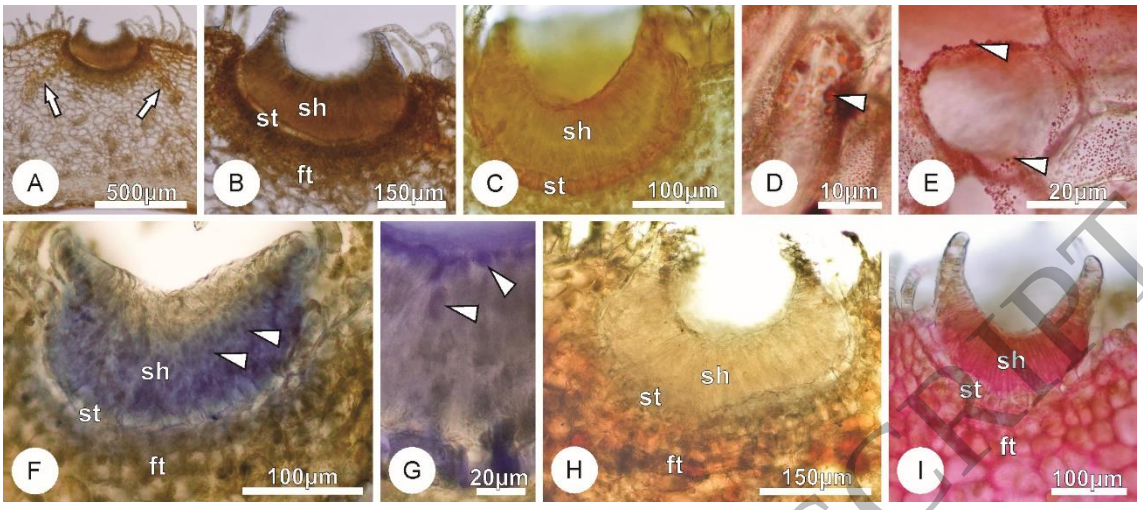


*Figure 8*
*150x66 mm ( x DPI)*

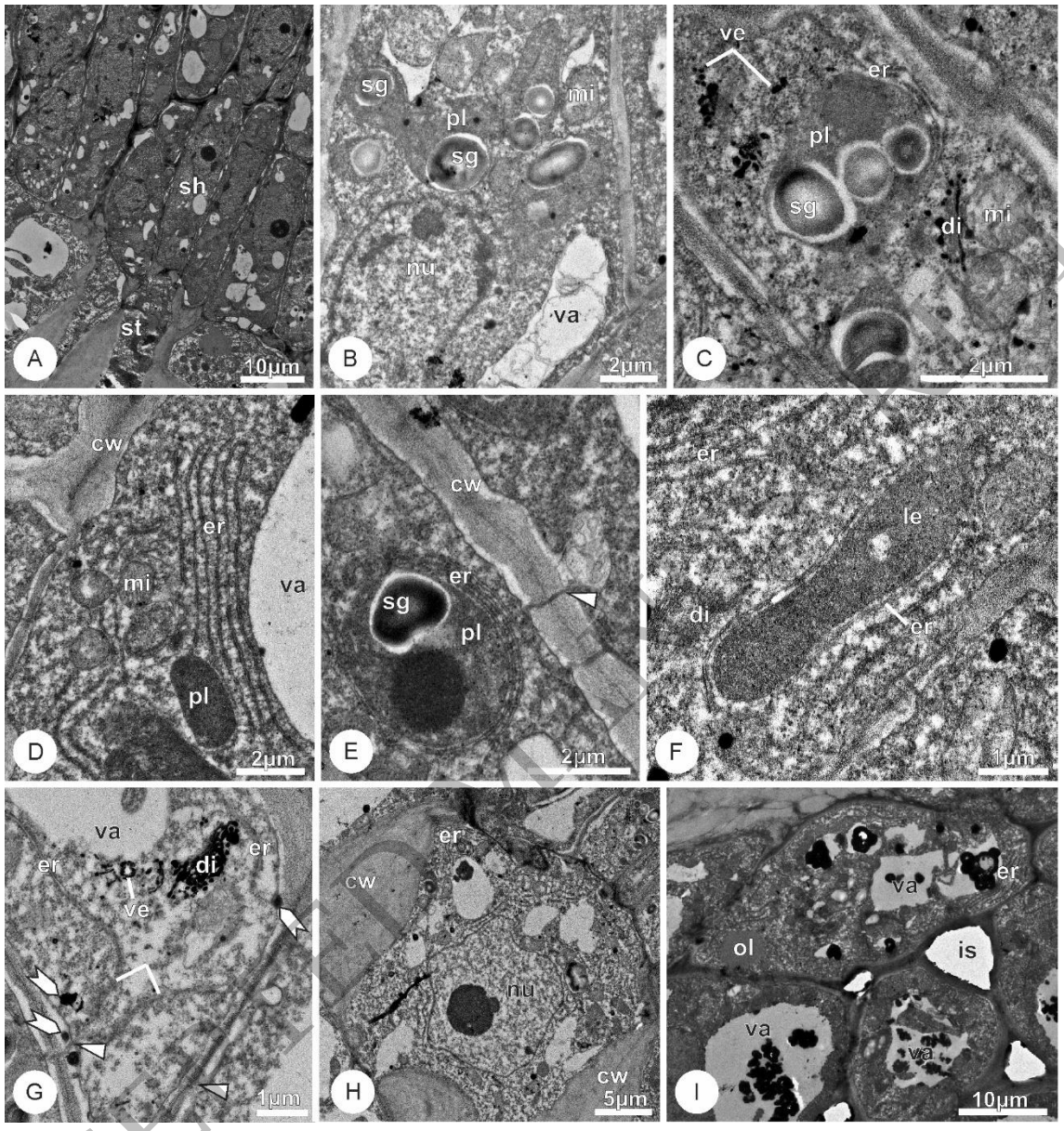


*Figure 9*
*150x159 mm ( x DPI)*

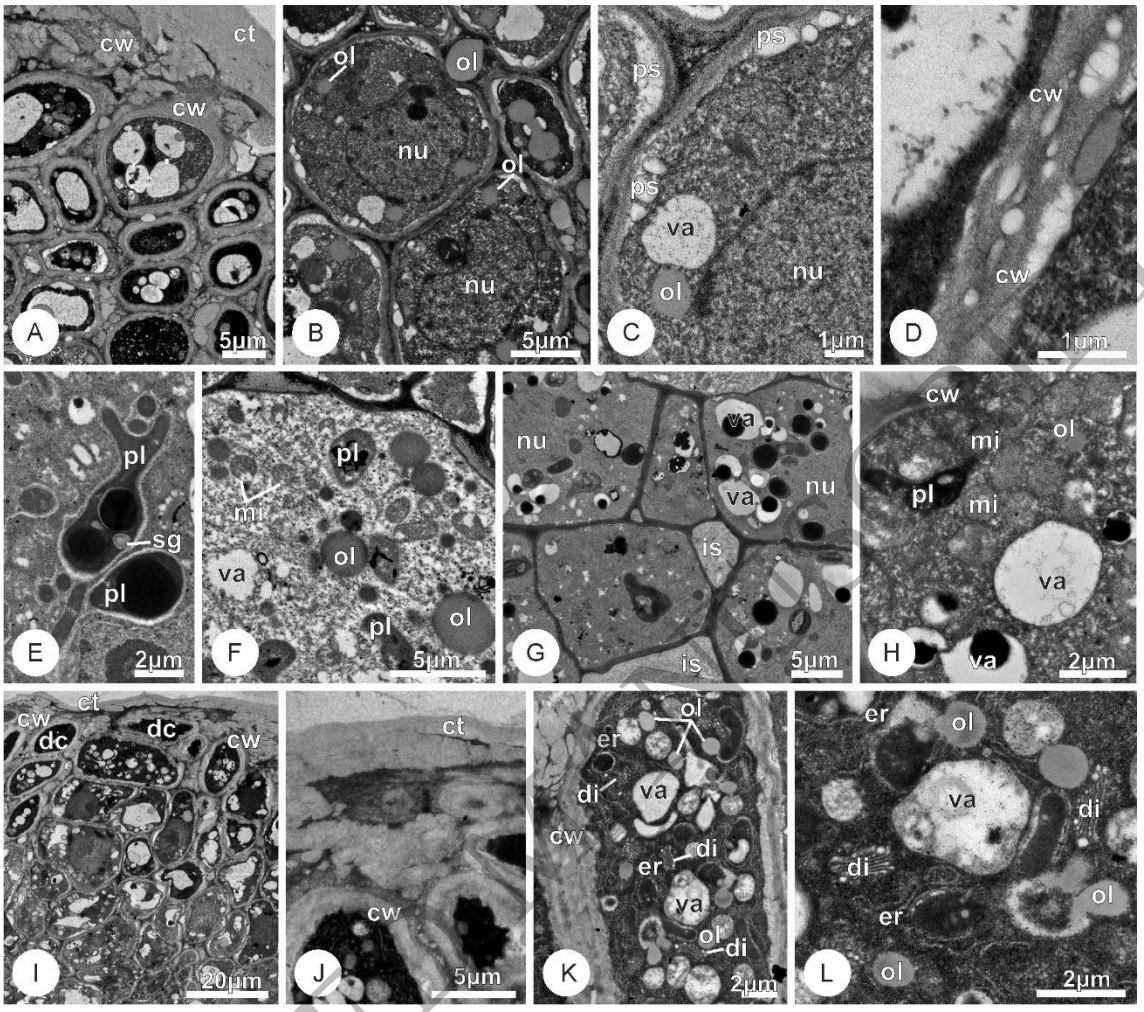


*Figure 10*
*150x132 mm ( x DPI)*